NAVAL POSTGRADUATE SCHOOL

MONTEREY, CALIFORNIA

THESIS

AN IMPROVED THERMAL BLOOMING MODEL FOR THE LASER PERFORMANCE CODE ANCHOR

by

Joseph C. Collins

June 2016

Thesis Advisor:	Keith R. Cohn
Second Reader:	Joseph Blau

Approved for public release; distribution is unlimited

THIS PAGE INTENTIONALLY LEFT BLANK

REPORT DOCUMENTATION PAGE

Form Approved OMB No. 0704-0188

1. AGENCY USE ONLY *(Leave blank)*	2. REPORT DATE June 2016	3. REPORT TYPE AND DATES COVERED Master's thesis	

4. TITLE AND SUBTITLE AN IMPROVED THERMAL BLOOMING MODEL FOR THE LASER PERFORMANCE CODE ANCHOR	5. FUNDING NUMBERS
6. AUTHOR(S) Joseph C. Collins	

7. PERFORMING ORGANIZATION NAME(S) AND ADDRESS(ES) Naval Postgraduate School Monterey, CA 93943-5000	8. PERFORMING ORGANIZATION REPORT NUMBER
9. SPONSORING /MONITORING AGENCY NAME(S) AND ADDRESS(ES) N/A	10. SPONSORING / MONITORING AGENCY REPORT NUMBER

11. SUPPLEMENTARY NOTES The views expressed in this thesis are those of the author and do not reflect the official policy or position of the Department of Defense or the U.S. Government. IRB Protocol number ____N/A____.

12a. DISTRIBUTION / AVAILABILITY STATEMENT Approved for public release; distribution is unlimited	12b. DISTRIBUTION CODE A

13. ABSTRACT (maximum 200 words)

Laser weapon systems, unlike conventional weapons, are heavily dependent upon the ever-changing atmospheric conditions in their employment theater. In order to understand the operational effectiveness of a laser weapon, the performance limits due to atmospheric conditions need to be understood. ANCHOR, a laser performance scaling code developed at the Naval Postgraduate School, is one such code used to model a laser's effectiveness for a variety of atmospheric conditions.

This thesis focuses on the calibration of ANCHOR's thermal blooming model. In the absence of turbulence, thermal blooming is generally well understood and the thermal blooming Strehl ratio is well defined. When turbulence is coupled with thermal blooming, however, the thermal blooming Strehl ratio is exceedingly difficult to quantify using scaling codes. This thesis calibrates ANCHOR's thermal blooming model using the full wave propagation code TBWaveCalc by adjusting the coefficients of an analytical formula to "best fit" the TBWaveCalc results over a wide variety of initial conditions.

14. SUBJECT TERMS thermal blooming, atmospheric propagation, laser, scaling code, Strehl ratio, ANCHOR, COAMPS, NAVSLaM, LEEDR	15. NUMBER OF PAGES 77
	16. PRICE CODE

17. SECURITY CLASSIFICATION OF REPORT Unclassified	18. SECURITY CLASSIFICATION OF THIS PAGE Unclassified	19. SECURITY CLASSIFICATION OF ABSTRACT Unclassified	20. LIMITATION OF ABSTRACT UU

THIS PAGE INTENTIONALLY LEFT BLANK

AN IMPROVED THERMAL BLOOMING MODEL FOR THE LASER
PERFORMANCE CODE ANCHOR

Joseph C. Collins
Lieutenant, United States Navy
B.S., The Citadel, 2010

Submitted in partial fulfillment of the
requirements for the degree of

MASTER OF SCIENCE IN APPLIED PHYSICS

from the

NAVAL POSTGRADUATE SCHOOL

June 2016

Approved by: Keith R. Cohn
                 Thesis Advisor

                 Joseph Blau
                 Second Reader

                 Kevin B. Smith
                 Chair, Department of Physics

THIS PAGE INTENTIONALLY LEFT BLANK

ABSTRACT

Laser weapon systems, unlike conventional weapons, are heavily dependent upon the ever-changing atmospheric conditions in their employment theater. In order to understand the operational effectiveness of a laser weapon, the performance limits due to atmospheric conditions need to be understood. ANCHOR, a laser performance scaling code developed at the Naval Postgraduate School, is one such code used to model a laser's effectiveness for a variety of atmospheric conditions.

This thesis focuses on the calibration of ANCHOR's thermal blooming model. In the absence of turbulence, thermal blooming is generally well understood and the thermal blooming Strehl ratio is well defined. When turbulence is coupled with thermal blooming, however, the thermal blooming Strehl ratio is exceedingly difficult to quantify using scaling codes. This thesis calibrates ANCHOR's thermal blooming model using the full wave propagation code TBWaveCalc by adjusting the coefficients of an analytical formula to "best fit" the TBWaveCalc results over a wide variety of initial conditions.

THIS PAGE INTENTIONALLY LEFT BLANK

TABLE OF CONTENTS

LIST OF FIGURES

THIS PAGE INTENTIONALLY LEFT BLANK

LIST OF TABLES

THIS PAGE INTENTIONALLY LEFT BLANK

LIST OF ACRONYMS AND ABBREVIATIONS

COAMPS	Coupled Ocean/Atmosphere Mesoscale Prediction System
DE	Directed Energy
DOD	Department of Defense
FEL	Free-electron Laser
HEL	High Energy Laser
LaWS	Laser Weapons System
LEEDR	Laser Environment Effects Definition and Reference
MIRACL	Mid-Infrared Advanced Chemical Laser
NACL	Navy-ARPA Chemical Laser
NAVSLaM	Navy Atmospheric Vertical Surface Layer Model
NPS	Naval Postgraduate School
SSL	Solid-State Laser

THIS PAGE INTENTIONALLY LEFT BLANK

ACKNOWLEDGMENTS

I would like to thank my thesis advisor, Professor Keith Cohn, and my second reader, Professor Joseph Blau, for their insight and assistance in completing this thesis. I would also like to thank Dr. Conor Pogue for his help and guidance in completing the research for this thesis.

THIS PAGE INTENTIONALLY LEFT BLANK

I.   INTRODUCTION

The feasibility of using directed energy (DE) weapons in a combat environment has been studied extensively by the Department of Defense (DOD) for decades. In recent years the Navy has developed a shipboard laser weapons system (LaWS) and deployed it onboard the USS *Ponce* in the Persian Gulf for testing and evaluation. While this can be seen as a step toward fielding lasers and other DE weapons aboard Naval platforms, there are still several hurdles that must be overcome. One such issue is the ability to accurately predict an effective engagement range. Laser weapons are acutely sensitive to atmospheric changes in their employment area, especially in the maritime environment. In order for a laser to be effective as a defensive weapon, the operator needs to understand the potential limitations of the laser in any environment before employment. The ANCHOR laser performance code was developed by the Naval Postgraduate School (NPS) Physics DE Group to meet this need while being extremely fast and adaptable. Given initial laser parameters and atmospheric inputs from atmospheric modeling codes, ANCHOR can compute laser effectiveness in a matter of seconds. The scope of this thesis focuses on the ANCHOR code, particularly in how it models the effects of thermal blooming. Specifically, ANCHOR's thermal blooming model was calibrated against TBWaveCalc, a full diffraction code published by MZA, over a wide variety of initial conditions.

An outline of this thesis includes a brief discussion of directed energy weapons, an overview of laser codes including ANCHOR, and the thermal blooming calibration method and results.

THIS PAGE INTENTIONALLY LEFT BLANK

II.   OVERVIEW OF DIRECTED ENERGY (DE) WEAPONS

A.   HISTORY

Since the invention of the laser in the early 1960s, the military has been heavily invested in its maturation and potential for battlefield application. In 1971, the U.S Navy established a dedicated High Energy Laser (HEL) program office in order to study and develop HEL technology capable of defending naval vessels at sea from aerial threats like anti-ship cruise missiles. Early testing was centered on CO_2 gas dynamic laser technology, with a wavelength of approximately 10.6 μm, the highest power laser at the time [1]. In 1973, it was demonstrated for the first time, using a continuous wave deuterium fluoride (DF) laser, that chemical laser technology could be scaled to high powers. With an output wavelength of around 3.8 μm, chemical lasers immediately became a better option than CO_2 lasers for naval applications due to superior atmospheric propagation in the maritime environment [1].

The Navy-ARPA Chemical Laser (NACL) was the Navy's first attempt to assess the plausibility of using a chemical HEL for fleet defense using a scaled-up DF laser. In 1978, using the NACL, the Navy successfully demonstrated the ability to engage and destroy missiles in flight – specifically TOW anti-tank missiles flying at low altitude with crossing trajectories at high subsonic speeds [1]. Leveraging the knowledge gained from the NACL, the Navy set it sights on developing a laser capable of reaching much higher power levels, developing the megawatt class Mid-InfraRed Advanced Chemical Laser (MIRACL) in the early 1980s. Throughout the 1980s, MIRACL was used by the DOD for a variety of damage and vulnerability tests at the High Energy Laser System Test Facility at White Sands, New Mexico, ultimately, in 1989 demonstrating the capability of engaging a supersonic threat [1]. Despite the promising performance of chemical lasers, the Navy ultimately ceased its research citing logistical and safety issues associated with the hazardous chemicals in a shipboard environment.

As technology matured, the Navy began to focus on using Solid-State Lasers (SSLs) for shipboard applications, due to their increased propagation at shorter wavelengths, culminating in the deployment of the LaWS on the USS *Ponce* in 2014.

B.   ADVANTAGES

A major drive toward the use of HEL weapons has been their perceived advantage in combat, specifically when battling an asymmetric threat. One advantage is the ability to place a focused spot of light on a target instead of firing a projectile. The HEL beam can inflict a varying amount of thermal damage on target, delivering a high amount of energy to a localized target, thus minimizing collateral damage and increasing mission kill effectiveness. The HEL weapon can begin delivering energy to the target almost instantly—at the speed of light—ideal for long-range targets and when a quick reaction is necessary to combat the threat. As an electric weapon, the magazine is only limited by the available power onboard, so the weapon can conduct multiple shots without the need to reload, and the cost per shot is equivalent to the cost of the fuel required to produce the power. Along with these advantages, there are currently several issues that could limit their effectiveness. The weapon requires the target to be in line of sight; it cannot engage targets over the horizon or low-flying threats obscured by waves. A finite dwell time is required to accrue damage (a typical engagement could last several seconds) limiting its ability to be used against simultaneous threats. An HEL weapon is also susceptible to atmospheric conditions and can be limited due to rain, haze, fog, or similar weather phenomena. As the technology matures, many of these disadvantages can be mitigated, making their advantages much more enticing.

C.   TECHNOLOGIES

The term laser stands for Light Amplification by Stimulated Emission of Radiation. By its nature, a laser increases or amplifies light waves after they have been generated by spontaneous emission. A laser generally consists of four components: laser pumping source, a gain or amplifying medium, total reflecting mirror, and partial reflecting mirror illustrated in Figure 1 [2].
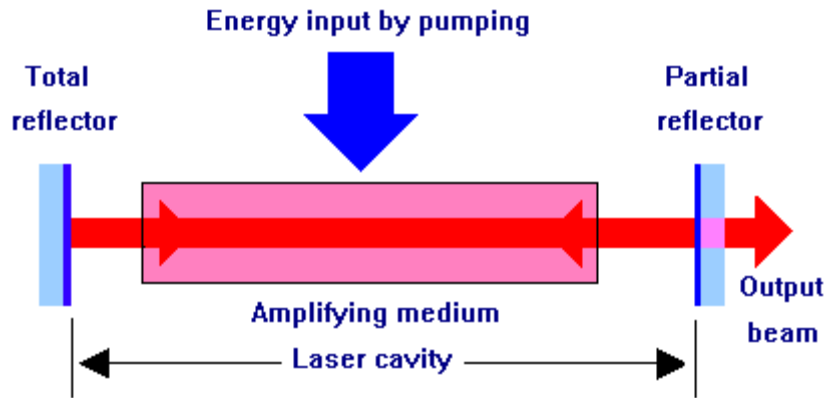
Figure 1. Example of solid state laser components

In recent years, naval research into HELs has centered on SSLs and Free-Electron Lasers (FELs). Vastly different systems, SSLs represent the best hope for attaining high powers today, while FELs represent the potential for high power, efficient lasers with a variety of military relevant applications for the future.

SSLs, which utilize solid-state materials as their gain medium, represent a large percentage of current HEL research. SSLs generally consist of crystalline or glass host materials with specific atomic ions—rare earth or transition-metal elements—grown into the host material to act as the lasing species (dopant ions). SSLs use optical pumping, either through diode-pumping or flashlamp-pumping, to create the population inversion necessary for the lasing process. Advantages of SSLs are their relative maturity, compact and lightweight design, and efficiency. For naval applications, SSLs are particularly enticing due to their lack of harmful bi-products such as hazardous chemicals or ionizing radiation, and due to the fact that they output wavelengths that propagate extremely well in clear weather, particularly Ytterbium lasers with wavelengths of approximately 1 μm. Unfortunately, there are several potential barriers to their full-scale use in military applications. Of particular note is the fact that the glass/crystalline host materials generally have a low thermal conductivity, which would limit their average power output due to an inability to eliminate waste heat. A related issue is that in order to be effective as an HEL weapon, many SSLs must be combined, which can limit beam quality or increase the complexity of the laser system.

Free Electron Lasers generate light by sending a relativistic beam of electrons through a periodic magnetic field. As these free electrons move through vacuum, the magnetic field causes them to undulate and therefore produce light. There are two types of FELs, oscillator FELs and amplifier FELs. An oscillator FEL is made up of three core elements: an electron beam and the accelerator to produce it, the undulator magnet, and an optical resonator. Amplifier FELs utilize a seed laser source in place of an optical resonator [3]. As the technology matures, the use of FELs as a HEL weapon becomes increasingly advantageous. Unlike other types of lasers, FELs are tunable and can vary the output wavelength for best atmospheric transparency. FELs are also naturally scalable and can potentially vary output power from the kW to MW levels depending on the target. Unlike the current configurations for SSLs, FELs can have excellent beam quality even at high power. Unfortunately for FELs, there are currently several roadblocks to their implementation onboard naval platforms: FELs are generally large (on the order of 20 m in length), heavy, and expensive, requiring large research teams to operate and maintain [3]. The technology is not yet mature enough for military applications.

D. LAWS AND PONCE

The Laser Weapons System was developed to test the capabilities and feasibility of solid-state lasers onboard naval platforms. LaWS was designed primarily as a cost effective defense against a swarm threat, small drones, or fast-attack craft in the water. The LaWS demonstrator incoherently combines several commercial off-the-shelf fiber SSLs, each with a power of abut 5 kW and a total power of approximately 30 kW, a beam quality factor, M^2, of 17, and a wavelength of 1.064 μm [4]. In the summer of 2014 LaWS was installed on the Afloat Forward Staging Base, USS *Ponce*, for a 12-month demonstration in a combat relevant, maritime environment. Prior to its deployment on the *Ponce*, LaWS had multiple successful tests, including successful engagements at NAWCWD China Lake, and maritime engagements off the coast of Southern California onboard the USS *Dewey* [4]. Following the demonstration period onboard *Ponce*, the LaWS system was cleared to remain in place for the foreseeable future as an operational asset, and is currently being used for daily target identification and watch stander training. The success of the LaWS systems has paved the wave for the Solid-State Laser

– Technical Maturation program, which has the goal of operationally fielding a 100 kW laser on surface combatants within the next five years.

THIS PAGE INTENTIONALLY LEFT BLANK

III. OVERVIEW OF ATMOSPHERIC CODES

A. ANCHOR

The NPS laser performance code, ANCHOR, is a MATLAB script that rapidly can explore millions of different initial condition combinations. ANCHOR has been calibrated against WaveTrain, an industry-developed full diffraction code that has been validated against existing codes that have been found to be in agreement with theory and experimentation [5]. ANCHOR produces results that are in approximate agreement with WaveTrain, but ANCHOR runs many orders of magnitude faster than WaveTrain. Unlike full diffraction codes like WaveTrain, which solve the paraxial wave equation numerically and provide irradiance profile information for each time step, ANCHOR uses well-known, experimentally validated analytical scaling laws to provide time-averaged values of irradiance, power-in-the-bucket, and other figures of merit.

Currently, there exist several variations of the ANCHOR code—S, L, and P— depending upon the desired results. ANCHOR S, the simplest version, assumes the atmospheric conditions, including the effects of turbulence, the total extinction, and the wind speed and direction remain constant along the beam path of the laser. Since the atmospheric conditions remain constant, ANCHOR S does not need output from atmospheric modeling codes; instead, the user specifies the atmospheric conditions for each study directly in the script. Based on the user defined input values, ANCHOR S outputs the time-averaged irradiance, time-averaged power-in-the-bucket, and dwell time.

The L and P versions allow the atmospheric parameters to vary along the beam path and therefore require output from atmospheric modeling codes in order to obtain this information. ANCHOR L and P both output 2D slices through the 3D engagement volume of the time-averaged irradiances, time-averaged powers-in-the-bucket, and dwell times.

ANCHOR L provides a horizontal slice for each figure of merit, showing changes in laser performance with varying altitude and range along a constant bearing from the laser platform. Instead of horizontal slices, ANCHOR P provides vertical slices from a

frame of reference above the platform, highlighting propagation changes with varying range and bearing for a constant altitude. Combined together as shown in Figure 2, the L and P outputs provide a complete picture of the engagement window.
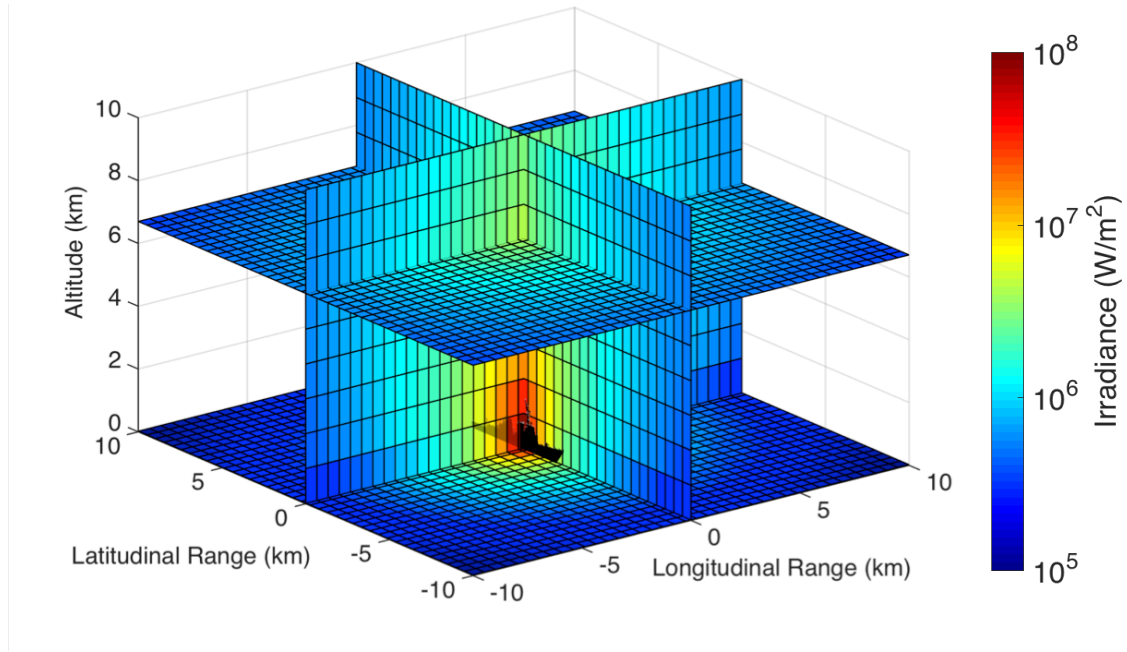
Peak irradiance vs target altitude, latitudinal and longitudinal range, with laser source at the origin.

Figure 2. ANCHOR 3D engagement volume

Whichever version of ANCHOR is used, the user defines inputs such as target height, platform height, laser diameter at the source (specifically, the 1/e diameter of the irradiance for a Gaussian beam, or the full diameter for a uniform beam), wavelength, laser output power, beam quality, beam type (Gaussian or uniform), and the root-mean-square total angular jitter. In order to find power-in-the-bucket, the user must define a bucket radius that typically corresponds to the desired damage spot size on the target. For dwell times, the user must input relevant properties that characterize target vulnerability, such as the amount of energy needed to melt the target area, any power loss mechanisms that remove energy from the target area, and fractional absorption of the target at the laser

10

wavelength. In addition to the user defined properties, atmospheric data for ANCHOR versions L and P must be loaded into the MATLAB environment from a code such as LEEDR (the Laser Environmental Effects Definition and Reference, developed by the Air Force Institute of Technology Center for Directed Energy), NAVSLaM (the Navy Atmospheric Vertical Surface Layer Model, developed by the Meteorology department of the Naval Postgraduate School), or COAMPS (the Coupled Ocean/Atmosphere Mesoscale Prediction System, developed by the Marine Meteorology Division of the Naval Research Lab). This study utilizes all three atmospheric codes.

1. ANCHOR Methodology

ANCHOR utilizes the following equation to calculate time-averaged irradiance $\langle I \rangle$ at the target:

$$\langle I \rangle = \frac{P_o \exp\left(-\int \varepsilon(z)dz\right)}{\pi \langle w_{tot} \rangle^2} \cdot S_{TB}, \tag{1}$$

where P_o is the output power of the laser at the beam director, z is the distance coordinate along the path from the beam director to the target, ε is the total extinction coefficient (i.e., the combination of the effects of absorption and scattering) provided by the atmospheric modeling code, $\langle w_{tot} \rangle$ is the time-averaged spot radius (1/e in irradiance) on target, and S_{TB} is the thermal blooming Strehl ratio.

In order to estimate power-in-the-bucket for a given bucket radius r_{BKT}, the following equations are used:

$$P_{BKT} = \begin{cases} \pi \cdot \langle I \rangle \cdot r_{BKT}^2 & if \quad r_{BKT} < w_{eff} \\ \pi \cdot \langle I \rangle \cdot w_{eff}^2 & if \quad r_{BKT} > w_{eff} \end{cases}. \tag{2}$$

Here, w_{eff} is the effective spot radius on target and is the result of the increase in spot size due to thermal blooming. It is calculated by dividing the time-averaged spot radius on target due to linear effects only, $\langle w_{tot} \rangle$, by the square root of the thermal blooming Strehl ratio,

11

$$w_{eff} \equiv \frac{\langle w_{tot} \rangle}{\sqrt{S_{TB}}} \quad . \tag{3}$$

In order to calculate dwell time to melt a certain volume of the target, ANCHOR uses the following equations:

$$P_{melt} = F_{ABS} \cdot P_{BKT} - P_{loss} \tag{4}$$

$$t_{dwell} = \frac{Q_{melt}}{P_{melt}} \quad . \tag{5}$$

In this case, F_{ABS} is the fractional target absorption; P_{melt} is the power available after subtracting parasitic losses due to conduction and radiation, which depends on the emissivity and thermal conductivity of the target material; and Q_{melt} is the amount of energy to melt a certain volume of the target and depends upon the target's material properties, specifically, the melting temperature, heat capacity, and heat of fusion.

a. Time-averaged spot radius on target

There are several contributions to the spot size of a laser beam on a target, including diffraction, turbulence, jitter, and thermal blooming. Thermal blooming is a non-linear effect that is accounted for by the S_{TB} factor in equation 1 and will be discussed in greater detail in another chapter. The other three effects contribute to the overall time-averaged spot size by (approximate) addition in quadrature [6]:

$$\langle w_{tot} \rangle^2 = w_d^2 + w_t^2 + w_j^2 \quad , \tag{6}$$

where w_d is the radius of the laser beam at the target solely due to diffraction in a vacuum, w_t is the radius solely due to turbulence-induced beam spreading, and w_j is the root-mean-square radius due to the angular jitter.

For a laser beam in a vacuum, the time-averaged spot radius is only a function of diffraction and w_d represents the ideal spot radius for a given range and known beam quality. The focus spot of a laser beam in a vacuum can be calculated by the following equation [6]:

$$w_d = M^2 \frac{2l}{kD} \quad \text{(Gaussian)}. \tag{7}$$

12

Here, M^2 is a measure of the beam quality of a laser, l is the range from the laser source to the target, and $k = 2\pi/\lambda$ is the wavenumber. For a Gaussian beam, D is equal to the 1/e diameter of the irradiance at the source. In the case of a uniform beam, where D is equal to the full diameter of the irradiance at the source, equation 7 becomes:

$$w_d = M^2 \frac{4l}{kD} \text{ (Uniform).} \tag{8}$$

ANCHOR utilizes the simplified equations to determine the diffraction-limited spot radius when calculating the time-averaged spot radius on target.

Outside a vacuum, the presence of atmospheric turbulence plays a role in the overall time-averaged spot radius as shown in equation 6. Turbulence-induced spreading of laser beams is generally caused by small-scale turbulent horizontal motion in the atmosphere that results from vertical temperature and density differences, wind shear, and convective air flow [3]. These atmospheric effects cause changes in the refractive index of the air along the path and in turn cause the beam to spread and the time-averaged irradiance to decrease. Many studies have been conducted in order to quantify electromagnetic wave propagation through turbulent media; of particular note is the work done by Fried that led to the development of the Fried parameter r_o, which can be used to describe the effects of turbulence on laser propagation [7]. The Fried parameter defines the diameter over which a laser beam can maintain transverse coherence throughout its propagation distance. Typical values of r_o are on the order of a few centimeters where smaller values correspond to stronger turbulence. To calculate r_o, the following equation is commonly used [8]:

$$r_o = 2.10[1.45k^2 \int_0^l C_n^2(z)(1-\frac{z}{l})^{\frac{5}{3}}dz]^{-\frac{3}{5}} \text{ (Spherical Wave).} \tag{9}$$

Here, k is the wavenumber, l is the distance from laser source to target, and C_n^2 is the refractive structure constant. The C_n^2 value was first theoretically parameterized by Kolmogorov and is experimentally measured; higher C_n^2 values are associated with stronger turbulence, and it is generally a function of altitude with larger C_n^2 occurring near the surface [3].

13

Plot A in Figure 3 shows a full diffraction simulation of a laser propagating over a range of 5 km in weak turbulence, $C_n^2 \approx 10^{-18}\,\mathrm{m}^{-2/3}$; here, the beam maintains transverse coherence throughout the propagation path so the result is a circular spot at the focus. Plot b in Figure 3, shows the beam propagation over a range of 5 km in stronger turbulence, $C_n^2 \approx 10^{-14}\,\mathrm{m}^{-2/3}$, and the resulting spot begins to break up into beamlets and spread out. The intensity at the focus is denoted by a color scale, with red indicating the highest peak irradiance and blue indicating the lowest.

a.) Weak turbulence, $C_n^2 \approx 10^{-18}\,\mathrm{m}^{-2/3}$ b.) Strong turbulence, $C_n^2 \approx 10^{-14}\,\mathrm{m}^{-2/3}$
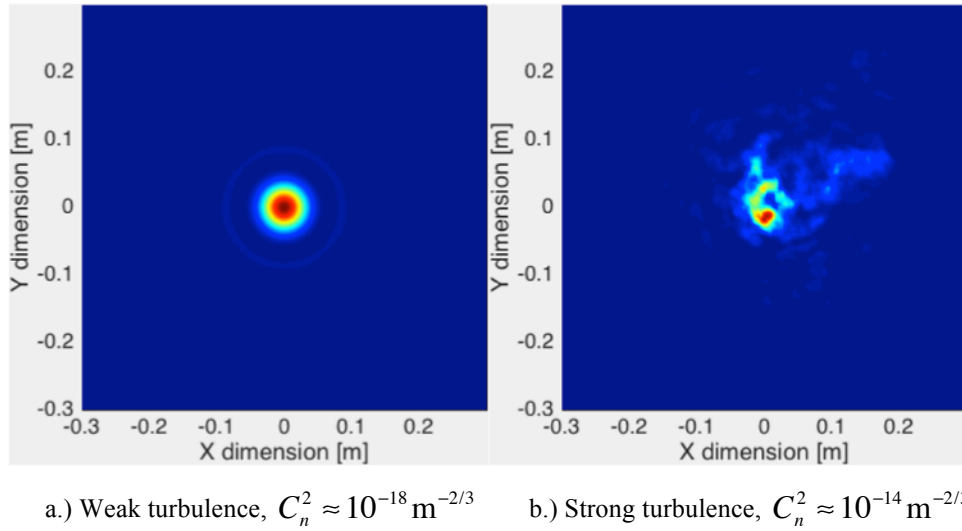
Figure 3. Laser diffraction simulation for strong and weak turbulence

Once the Fried parameter has been calculated by ANCHOR using the C_n^2 profile from the atmospheric modeling code, the turbulence-induced beam spreading can be calculated using the following equation [8]:

$$w_t = \frac{w_d}{M^2}\frac{D}{r_o}\ .$$

(10)

Here, w_t represents the contribution to the spot size from the total turbulence, including the effects of both long and short-term turbulence. The total turbulence term is used in the calculation of the time-averaged spot radius on target.

The spatial width due to jitter, w_j, has a varying effect on the time-averaged spot radius. The factors that contribute to the overall jitter are platform motion, and tracking error [8]. The beam jitter can be calculated with the following equation [6]:

$$w_j = \theta_{rms} l .$$ (11)

where θ_{rms} is defined as the effective angular jitter from all sources.

b. *Thermal Blooming Strehl Ratio*

Thermal blooming is a nonlinear propagation effect resulting from the absorption of laser radiation by molecules and aerosols in the atmosphere that alters the air density along the propagation path. The thermal blooming Strehl ratio, S_{TB}, is the ratio of the laser's irradiance with thermal blooming to the laser's irradiance without thermal blooming; therefore, S_{TB} ranges from ~0 (for strong thermal blooming) to ~1 (for weak thermal blooming). Depending on the laser output power and the propagation range, thermal blooming can become the dominant factor in determining laser effectiveness. How ANCHOR calculates S_{TB} will be discussed in the following chapter.

B. NAVY ATMOSPHERIC VERTICAL SURFACE LAYER MODEL (NAVSLaM)

NAVSLaM is a model developed by the Meteorology Department at NPS and is used by the Navy to calculate turbulence $\left(C_n^2 \right)$ profiles over the ocean up to approximately 100 meters above sea level. NAVSLaM takes numerical weather prediction model forecasts i.e. from COAMPS; weather data sets from sources like NOAA and NAVMETOCCOM; or real-world observations of the wind speed, air and sea temperatures, relative humidity, and pressure data; and outputs near-surface vertical modified C_n^2 profiles [9]. In order to calculate these profiles, NAVSLaM utilizes the Monin-Obukhov similarity theory, which assumes that within the surface layer conditions are horizontally homogenous and stationary, and that sensible heat, latent heat, and turbulent fluxes of momentum do not vary with height [10]. When blended with models such as COAMPS and LEEDR that calculate the upper-air refractivity profiles, a profile

of the turbulence in the entirety of the engagement window can be obtained and imported into ANCHOR to determine laser effectiveness.

In the maritime environment, the main source of turbulence in the surface boundary layer is the air/sea temperature difference. When the temperature of the air is less than the temperature of the sea, $T_{air} < T_{sea}$, the conditions are unstable, and there tends to be higher turbulence at the surface, which then rapidly decreases with altitude. When the temperature of the air is greater than the temperature of the sea, $T_{air} > T_{sea}$, the conditions are stable, there tends to be less turbulence at the surface, and it tends to remain relatively constant up to a few tens of meters above the surface.

In Figure 4, the wind speed is 1.9 m/s, the sea temperature is 90°F, the relative humidity is 80%, and the pressure is 10^5 Pa at 1 m. The figure shows C_n^2 profiles, up to 20 m, highlighting the difference between stable conditions, when $\Delta T > 0$ (red lines), unstable conditions, when $\Delta T < 0$ (green lines), and a neutral case, when $\Delta T = 0$ (black line). Where $\Delta T = T_{air} - T_{sea}$. This plot was generated using NAVSLaM.
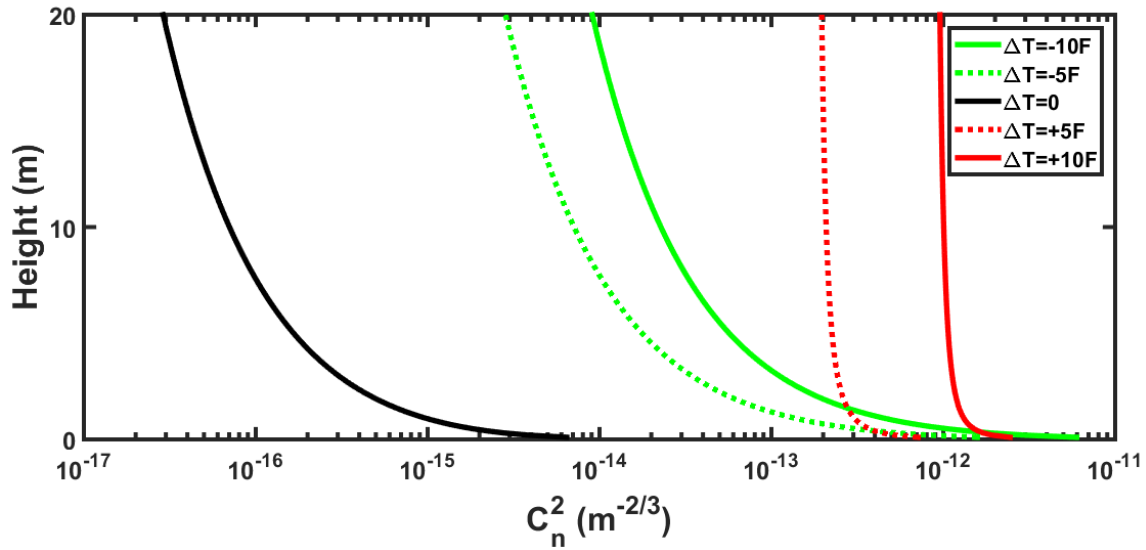

Figure 4. NAVSLaM output of C_n^2 vs. height for different air/sea temperature differences in the marine base layer

16

C. THE LASER ENVIRONMENTAL EFFECTS DEFINITION AND REFERENCE (LEEDR)

LEEDR, developed by the Air Force Institute of Technology Center for Directed Energy, is used to develop an atmospheric profile for a defined location. LEEDR utilizes input parameters like the season, time of day, and relative humidity to calculate profiles of "temperature, pressure, water vapor content, optical turbulence, atmospheric particulates, and hydrometeors as they relate to layer transmission and path/background radiance at any wavelength" for the defined location from the surface to an altitude of 100 km [11]. In order to calculate atmospheric profiles, LEEDR uses surface weather models based on the season and time of the day in order to define the atmospheric boundary layer. From this, LEEDR "computes the radiative transfer and propagation effects from the vertical profile of meteorological variables," providing the capability to create realistic atmospheric profiles for a specified location [11]. The LEEDR atmospheric profiles can then be exported to ANCHOR and used to model the laser's propagation in the maritime environment.

D. COUPLED OCEAN/ATMOSPHERE MESOSCALE PREDICTION SYSTEM (COAMPS)

COAMPS, developed by the Naval Research Lab Marine Meteorology Division, is used to predict atmospheric conditions. COAMPS predicts wind, temperature, pressure, clouds, and aerosols based on inputs from meteorological observations, satellite data, ship reports, ocean observations, and bathymetry [12]. Because COAMPS calculates its initial state based on observations, it is re-locatable and can be used worldwide. The COAMPS forecast data can also be input into NAVSLaM to calculate the refractivity profile near the surface. When the two models are blended together, an accurate model for the engagement window can be imported into ANCHOR to determine laser effectiveness in a quasi-real-world environment.

E.   LASER PROPAGATION EXAMPLE: LEEDR

As an example, using a laser with properties highlighted in Table 1 and atmospheric data for the Taiwan Straits during the winter obtained from LEEDR, ANCHOR outputs the figures of merit shown in Figures 5–10.

Table 1.   ANCHOR example, laser parameters

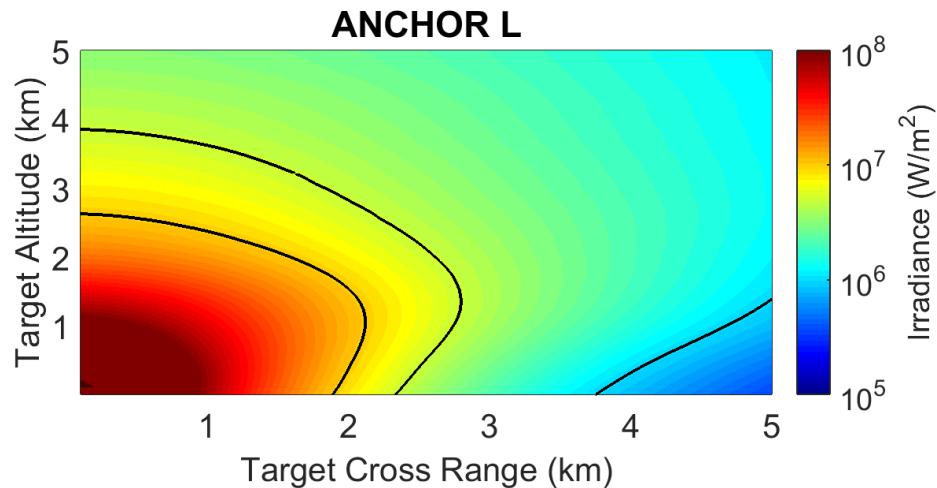| Laser Parameters	
Laser Power (kW)	100
Wavelength (μm)	1.064
Beam Quality	$M^2=3$
RMS Jitter (μrad)	5
Beam Director Diameter (m)	0.3
Beam Type	Uniform
Beam Director Height (m)	10

Figure 5. ANCHOR: Time-averaged irradiance vs. target range and altitude, for a 100 kW laser

The L variation of ANCHOR outputs an irradiance curve for the propagation path along a constant bearing from platform to target (in this example 90°), with varying range and altitude. The color scale on the right of the figure highlights the irradiance on target. In Figure 5, the platform is located at the origin, which is also the region with highest irradiance on target. The black contour lines correspond to irradiance thresholds, and represent the relative hardness of a target. The contour line closest to the platform corresponds to an irradiance of 10 MW/m^2, and would be associated with a harder target. The contour line farthest to the right of the platform corresponds to an irradiance of 1 MW/m^2 and would be associated with a softer target. The contour line in the center corresponds to an irradiance of 5 MW/m^2.

Like the L variation, the P variation of ANCHOR outputs an irradiance curve shown in Figure 6, however, the P variation outputs a curve of the propagation path for a constant altitude—for this example 10 m, with varying bearing and range.
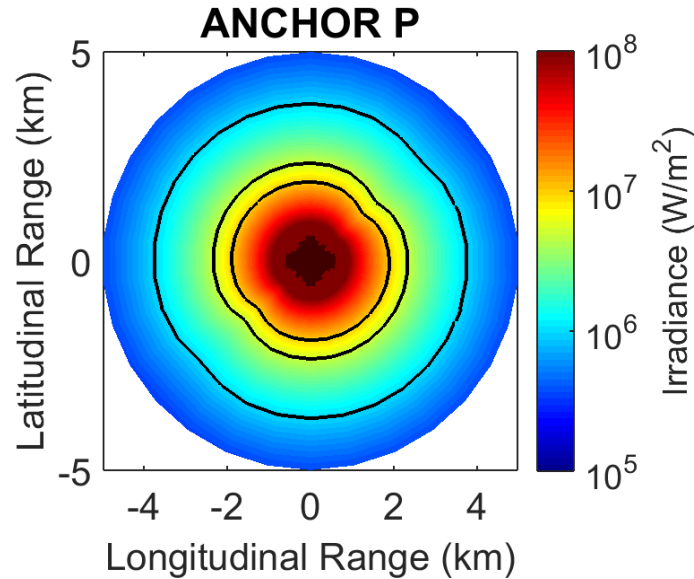

Figure 6. ANCHOR: Time-averaged irradiance vs. longitudinal range and latitudinal range, for a 100 kW laser

In Figure 6, the platform is at the center of the plot, the black contour lines represent the same irradiance thresholds as Figure 5.

19

In order to calculate power-in-the-bucket, a bucket size must be identified. Figures 7 and 8 are for a bucket radius of 5 cm.
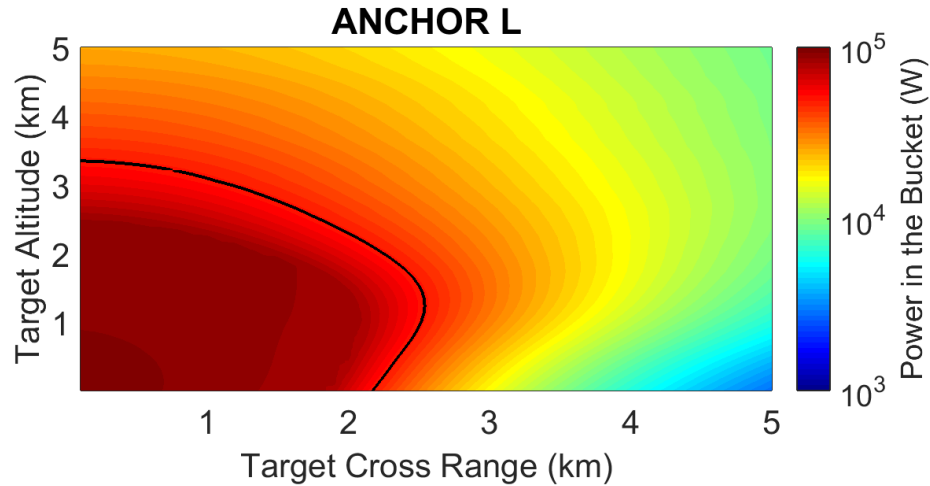

Figure 7. ANCHOR: Power-in-the-bucket vs. target range and altitude for a 100 kW laser

Figure 7 is the ANCHOR L output for power-in-the-bucket. The curve shows that close to the platform—at the origin—most of the laser power falls in the bucket. As range and altitude increase, less power falls in the bucket. The contour line represents a threshold of 50 kW.

Similarly, Figure 8 shows the ANCHOR P output of power-in-the-bucket for the same criteria.
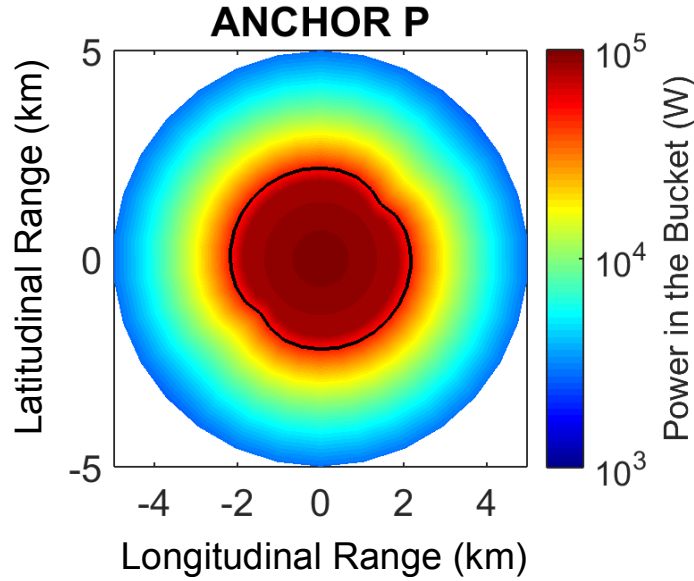
Figure 8. ANCHOR: Power-in-the-bucket vs. longitudinal range and latitudinal
range, for a 100 kW laser

Figure 8 shows that at the platform, near the center of the plot, the power-in-the-bucket exceeds the threshold value and as the radius around the platform increases less power falls in the bucket.

In order to calculate required dwell time for hard kill of a given target, several material properties for the target are used to calculate Q_{melt}, F_{ABS}, and P_{loss}, discussed previously in the ANCHOR methodology section. For this example a hard kill is defined as melting a 5 cm radius, 3 mm thick piece of aluminum, Q_{melt} for the aluminum is approximately 50 kJ, P_{loss} is approximately 2.5 kJ, and F_{ABS} is 15%. Using these values ANCHOR produces the dwell time plots shown in Figures 9 and 10:
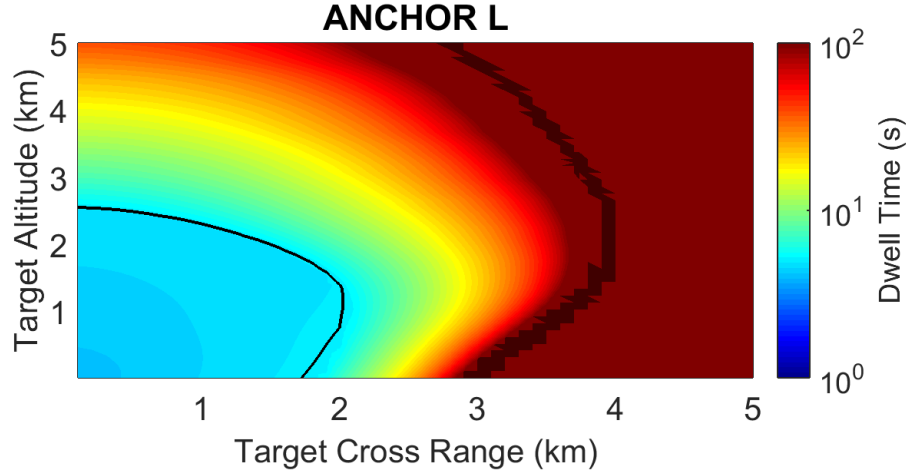
ANCHOR L

Plot of required dwell time for hard kill of a 100 cm², 3 mm thick piece of aluminum

Figure 9. ANCHOR: Required dwell time vs. target range and altitude, for a 100 kW laser

For the L variation of ANCHOR shown in Figure 9, the color scale represents required dwell times. The dark red is predominate after about 3 km on the horizontal axis and shows that for this distance the dwell time diverges because P_{melt}, the power available to melt the target, is much less than the P_{loss}, the power lost to conduction and radiative processes; the laser is ineffective at this range, at least for hard kills of this particular target. The black contour line in this case represents the dwell time threshold of 5 s and represents the maximum range for which a target with the parameters defined in this section can be destroyed in 5 s.
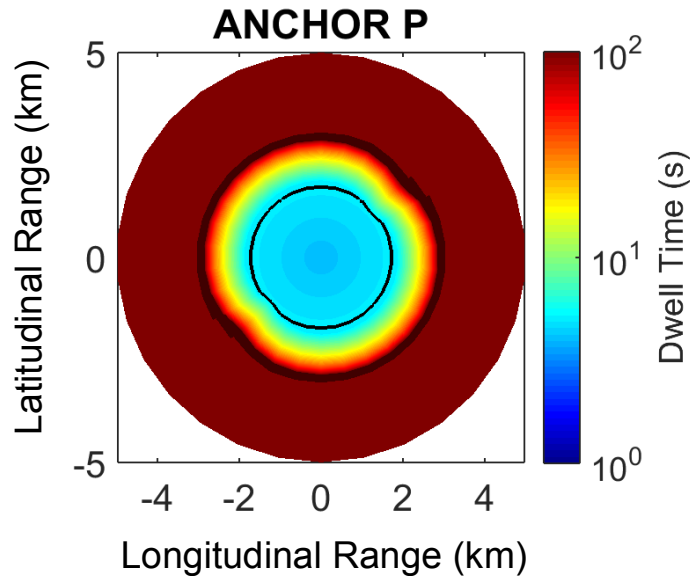
Figure 10. ANCHOR: Required dwell time vs. longitudinal range and latitudinal range, for a 100 kW laser

Figure 10 represents the same scenario for the P variation with an altitude of 10 m. The figure shows that, for an altitude of 10 m at a radius of approximately 3 km, the dwell time again diverges.

Comparing plots of irradiance, power-in-the-bucket, and dwell time, an operator of a laser weapons system can attain an accurate indication of the laser's effectiveness against a variety of targets in a matter of seconds, thus allowing the operator to make quick decisions regarding the tactical employment of the system.

F.   LASER PROPAGATION EXAMPLE: COAMPS/NAVSLaM

COAMPS can be used to obtain weather forecasting data. This data is blended with NAVSLaM and LEEDR to create an atmospheric profile that can be input into ANCHOR to determine laser effectiveness in a quasi-real world environment. As an example, atmospheric data was obtained from a COAMPS forecast for NSWC Dahlgren at 8 pm local time on 16 June 2014. The wind speed, air temperature, and wind heading predictions from COAMPS were then uploaded into NAVSLaM to obtain a turbulence

profile. Using extinction coefficients computed with LEEDR and the laser parameters defined in table 1, the COAMPS, NAVSLaM, and LEEDR profiles were blended and input into ANCHOR to produce the results shown in Figures 11–13.
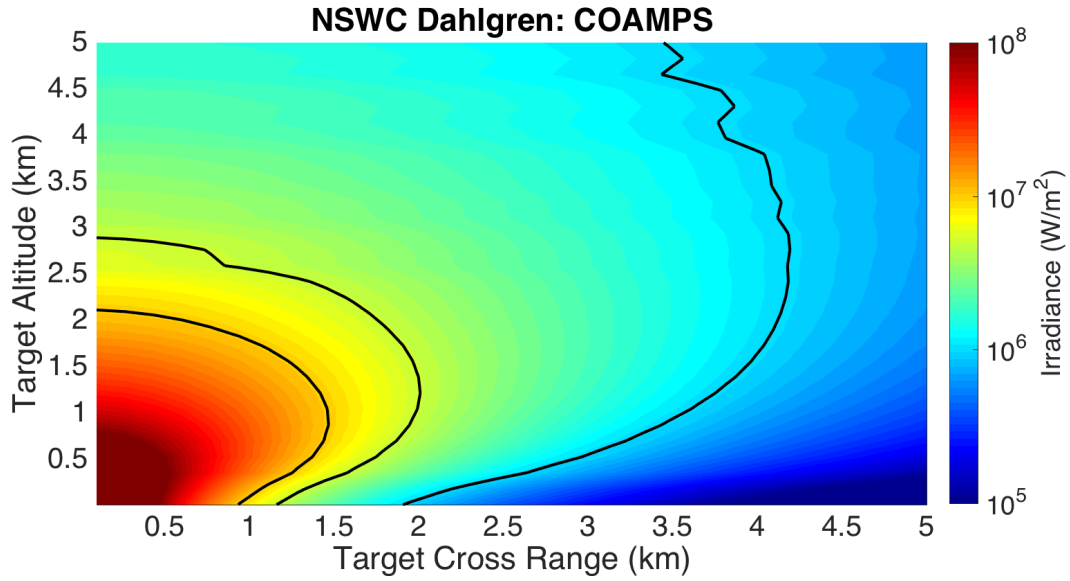

Figure 11. ANCHOR: Time-averaged irradiance vs. target range and altitude, for a 100 kW laser using COAMPS, NAVSLaM, and LEEDR
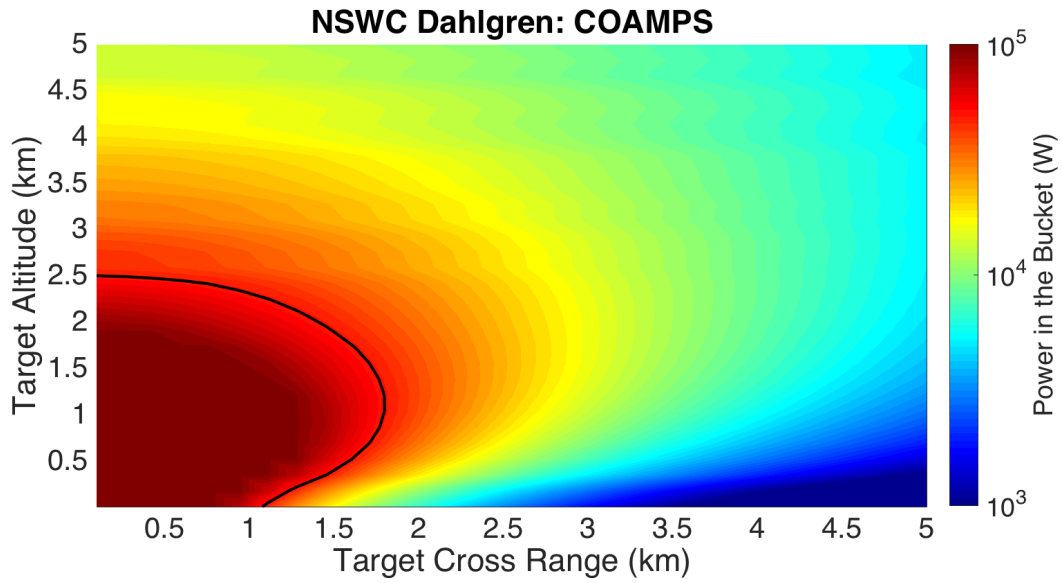
Figure 12. ANCHOR: Power-in-the-bucket vs. target range and altitude for a 100 kW laser, using COAMPS, NAVSLaM, and LEEDR
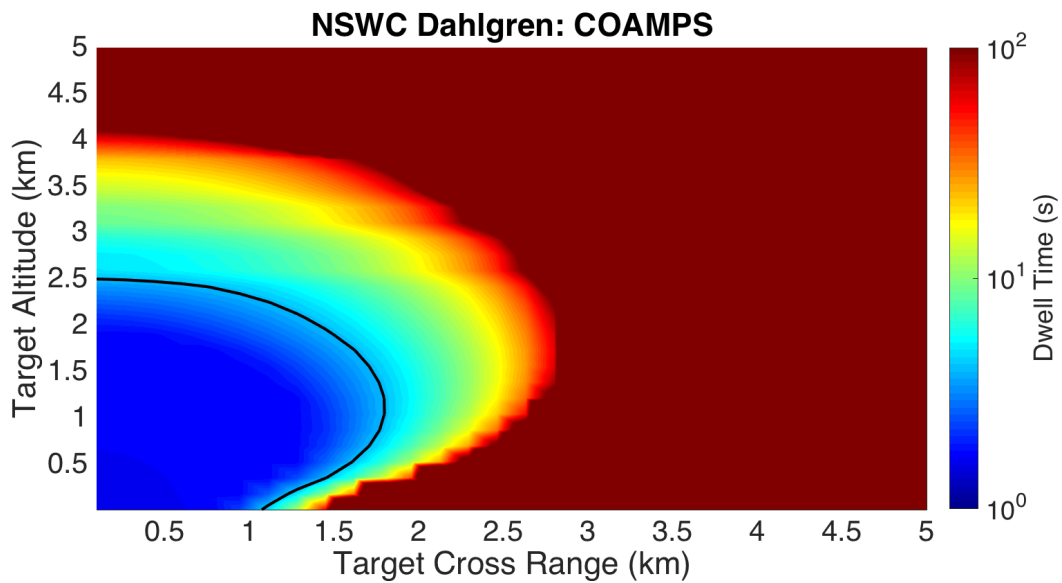

Figure 13. ANCHOR: Required dwell time vs. target range and altitude for a 100 kW laser, using COAMPS, NAVSLaM, and LEEDR

In each of the figures, a figure of merit is plotted against target range and altitude with the laser platform at the origin. The contour lines in Figure 11 represent threshold values of 10 MW/m^2 (contour closest to platform), 5 MW/m^2, and 1 MW/m^2 (contour furthest from platform). The contour lines pull in toward the platform at low altitudes due to high turbulence at the surface. The contour line in Figure 12 represents a power-in-the-bucket threshold of 50 kW, and appears to decrease rapidly in the horizontal direction at low altitude. Figure 13 shows the required dwell time plot with the dwell time threshold, 5 s, denoted by the black contour line. Figure 13 also shows that the required dwell time diverges beyond a range of 1 km at the surface due to the high turbulence.

Using the blend of COAMPS, NAVSLaM, and LEEDR for the atmospheric input into ANCHOR allows the operator to calculate a laser's effectiveness in near-real time, creating a more realistic assessment of operational employment.

IV. THERMAL BLOOMING

A. THERMAL BLOOMING OVERVIEW

Along the transmission path of a laser beam, the laser propagates through various absorbing media. As the beam passes through the media, thermal energy is transferred from the beam to the air, causing the air to heat up. This alters the air's density and therefore its index of refraction. These fluctuations cause the beam to spread out and distort [13]. Figure 14 highlights the effects of thermal blooming on the laser beam. The white contour represents 1/e of the peak irradiance. The left portion of the figure—the side view of the beam—shows the thermal blooming induced beam spreading after passing through an absorbing medium represented by a diverging lens denoted by the black line. The right portion of the figure is the transverse profile of the beam and shows that the effects of thermal blooming are most pronounced at the center of the beam, where a donut-shaped intensity pattern appears, due to the diverging lens.
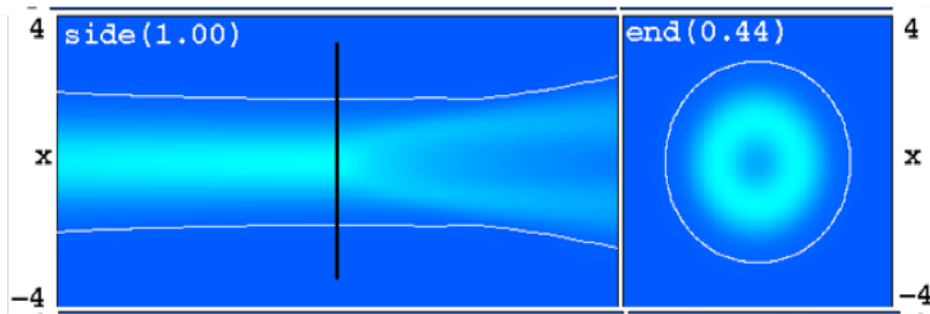

Figure 14. Laser diffraction simulation highlighting thermal blooming effects in the atmosphere

Understanding thermal blooming is important in calculating the time-averaged irradiance when studying laser weapons systems. The effects of thermal blooming become more pronounced at higher laser powers, especially in the maritime environment where there is generally higher absorption. Beyond a certain threshold power level, the thermal blooming becomes so severe that increasing the laser power will decrease the irradiance on target, potentially affecting the range of the laser.

B.   THERMAL BLOOMING THEORY

The diffraction of a laser along its propagation path is described by the paraxial wave equation:

$$\frac{\partial \psi}{\partial z} = -\frac{\varepsilon}{2}\psi + \frac{i}{2k}\nabla_\perp^2\psi + (ik\delta n)\psi,$$ (12)

where the irradiance is given by:

$$I = \frac{c\varepsilon_o}{2}\psi^*\psi.$$ (13)

Here, c is the speed of light in a vacuum, ε_o is the permittivity of a vacuum, and ψ is the complex laser field. Equation 12 incorporates the effects due to extinction, $-\frac{\varepsilon}{2}\psi$; the effects due to diffraction, $\frac{i}{2k}\nabla_\perp^2\psi$; and the effects due to turbulence and thermal blooming, $(ik\delta n)\psi$.

The δn component, where $\delta n = \delta n_{TB} + \delta n_{Turb}$, includes the changes in the refractive index from both turbulence and thermal blooming [13]. The thermal blooming contribution δn_{TB} represents the change in the refractive index n caused by the change in temperature of the air ΔT due to thermal blooming:

$$\delta n_{TB} = \frac{dn}{dT}\Delta T = -\frac{n_o-1}{T}\Delta T.$$ (14)

Here, n_o represents the initial index of refraction for the atmosphere and ΔT is calculated using the isobaric heating equation:

$$\frac{\partial \Delta T}{\partial t} = \frac{\alpha}{\rho C_p}I - \left(\vec{v}\cdot\vec{\nabla}_\perp\right)\Delta T + \left(\frac{K}{\rho C_p}\nabla^2\right)\Delta T.$$ (15)

Here, $\frac{\alpha}{\rho C_p}I$ includes the effects due to laser heating, where α is the atmospheric absorption coefficient, ρ is the air density, and C_p is the specific heat at constant pressure. The term $\left(\vec{v}\cdot\vec{\nabla}_\perp\right)\Delta T$ includes the effects due to convective heat transfer, where $\vec{v}$ is the wind velocity and $\vec{\nabla}_\perp$ is the transverse Laplacian. Essentially, the $\vec{v}\cdot\vec{\nabla}_\perp$ term

picks off the components of the wind velocity that are perpendicular to the beam path.

The term $\left(\dfrac{K}{\rho C_p} \nabla^2 \right) \Delta T$ includes the effects due to conductive heat transfer; typically, the

effects due to conduction are much smaller than those due to convection and can be ignored [14]. From Equation 15 it is important to note that ΔT depends on I (which is what we are trying to find) and I depends on δn (and, consequently, on ΔT). Therefore, in order to solve for I and ΔT, full diffraction codes solve Equations 12 and 15 numerically and iteratively along the beam path.

Deriving a numerical solution to these equations is time intensive, generally taking a full diffraction code minutes to hours to solve. In order to attain a solution in a fraction of the time, scaling codes typically fit a curve to the output from numerical diffraction codes. The form of the curve fit is usually:

$$ S_{TB} = \frac{1}{1 + AN_D^B} , \tag{16} $$

where, S_{TB} is the thermal blooming Strehl ratio discussed in the previous chapter, A and B are the fitting coefficients and N_D is the thermal blooming distortion number defined as:

$$ N_D = -\frac{4\sqrt{2}kP}{\rho C_p} \int \frac{\alpha(z)T(z)n_T(z)}{v(z)D(z)} dz . \tag{17} $$

Here, P is the laser power, z is along the path of the laser, $n_T = dn/dt = -(n_o - 1)/T_o$, v is the transverse wind speed, and D is the diameter of the beam. One of the issues with using N_D is that it is dependent upon the beam diameter, which itself depends on thermal blooming.

ANCHOR, a scaling code, uses a similar method to calculate the thermal blooming Strehl ratio, S_{TB} :

$$ S_{TB} = \frac{1}{1 + AN_{csw}^B N_F^C} , \tag{18} $$

where A, B, and C are fitting coefficients; N_{csw} is the weighted collimated distortion number defined as follows:

$$N_{csw} = \sum_z N_c(z)W(z),$$ (19)

where W is a weighting function, z is the path coordinate, and N_c is the collimated distortion number defined as follows:

$$N_c(z) = \frac{(n_o-1)\alpha(z)Pz^2}{\pi n_o \rho C_p T(z)v(z)D_o^3} .$$ (20)

Here, D_o is the beam diameter at the source. Because the effects of thermal blooming vary based upon where along the path the measurement is taken and upon the size of the beam diameter – peak thermal blooming tends to occur closer to the platform for smaller diameters – it is beneficial to multiply N_c by a weighting function given in [15]. The Fresnel number is derived from the following equation:

$$N_F = \frac{R_o}{w_{tots}} .$$ (21)

Here, R_o is the beam radius at the source and w_{tots} is defined as the spot size radius including only the effects of diffraction as defined in equations 7 and 8 from the previous chapter, short-term turbulence as discussed below, and jitter as discussed in the previous chapter. In weak turbulence, $r_o > D_o/3$, where r_o is the Fried parameter, the contribution due to short-term turbulence is given by [8]:

$$w_{ts} = \sqrt{0.182}\left(\frac{w_d}{M^2}\right)\left(\frac{D_o}{r_o}\right) .$$ (22)

For stronger turbulence, when $r_o < D_o/3$, the following equation is used:

$$w_{ts} = \frac{w_d}{M^2}\sqrt{\left(\frac{D_o}{r_o}\right)^2 - 1.18\left(\frac{D_o}{r_o}\right)^{\frac{5}{3}}} .$$ (23)

Because the beam wandering effects of long-term turbulence happen on a longer time-scale than the development of thermal blooming effects, the long-term turbulence contribution can be ignored when calculating thermal blooming. By replacing the total turbulence term, w_t with short-term turbulence in the spot radius equation from the previous chapter, w_{tots} can be calculated. Including N_F allows ANCHOR to account for the first order effects caused by turbulence, diffraction, and jitter into the Strehl ratio for a more physical representation of thermal blooming.

C. THERMAL BLOOMING CALIBRATION

TBWaveCalc, a script-driven atmospheric propagation tool, was used to determine the A, B, and C coefficients for the Strehl ratio from equation 18. TBWaveCalc is built into ATMTools and is developed by MZA. It is a full diffraction code that can model the path of a laser beam given the initial laser geometry and atmospheric conditions, and includes thermal blooming and combined turbulence effects [16].

In order to calibrate ANCHOR's thermal blooming Strehl ratio, TBWaveCalc was run for several thousand different laser and atmospheric parameters, consuming many thousands of hours of computer processing time. A MATLAB script was developed to generate the TBWaveCalc input files, analyze the output, and calculate N_c, N_{csw}, and N_F. The laser and atmospheric parameters were chosen to cover a wide variety of initial conditions and output powers. TBWaveCalc was run multiple times for a given atmosphere and laser geometry using different random seeds for the turbulence screens, and then the results were averaged.

The TBWaveCalc Strehl ratio was calculated from the ratio of peak irradiances after running the code with and without thermal blooming. The ANCHOR Strehl ratio was calculated using Equation 18 for the N_{csw} and N_F values obtained from MATLAB. Initial guesses for coefficients A, B, and C were used to calculate the initial value for the ANCHOR Strehl ratio. From the initial Strehl ratio, the inverse Strehl ratio was calculated and compared against the inverse Strehl ratio calculated from the TBWaveCalc results. The difference between the inverse Strehl ratios were tabulated in Excel and then summed together. The sum of differences was then input into the Excel solver function where, the A, B, and C coefficients were adjusted in order to minimize the sum of the differences. These coefficients were then incorporated into Equation 18 in order to calculate the "best fit" Strehl ratio for ANCHOR. The ANCHOR Strehl ratio was then plotted against the thermal blooming Strehl ratio calculated from TBWaveCalc and compared, as shown in Figures 15–43.

1. Results: Wind = 10 m/s, D = 30 cm, Range = 5 km

In order to see how ANCHOR's calibrated thermal blooming model compares to TBWaveCalc, the inverse Strehl ratios were plotted against each other for a variety of conditions. Since the Strehl ratio is a value between 0 and 1, the inverse Strehl ratio was plotted instead. Plotting the inverse Strehl ratios versus output power elucidates small differences between the results for strong thermal blooming, i.e., when $S_{TB} \ll 1$. In Figures 15–21, the inverse Strehl ratio is plotted against output laser power from 10 kW to 400 kW. The beam diameter at the source is 30 cm, the wind is a constant 10 m/s, and the range is 5 km. The blue line represents the ANCHOR data and the red points represent TBWaveCalc results.
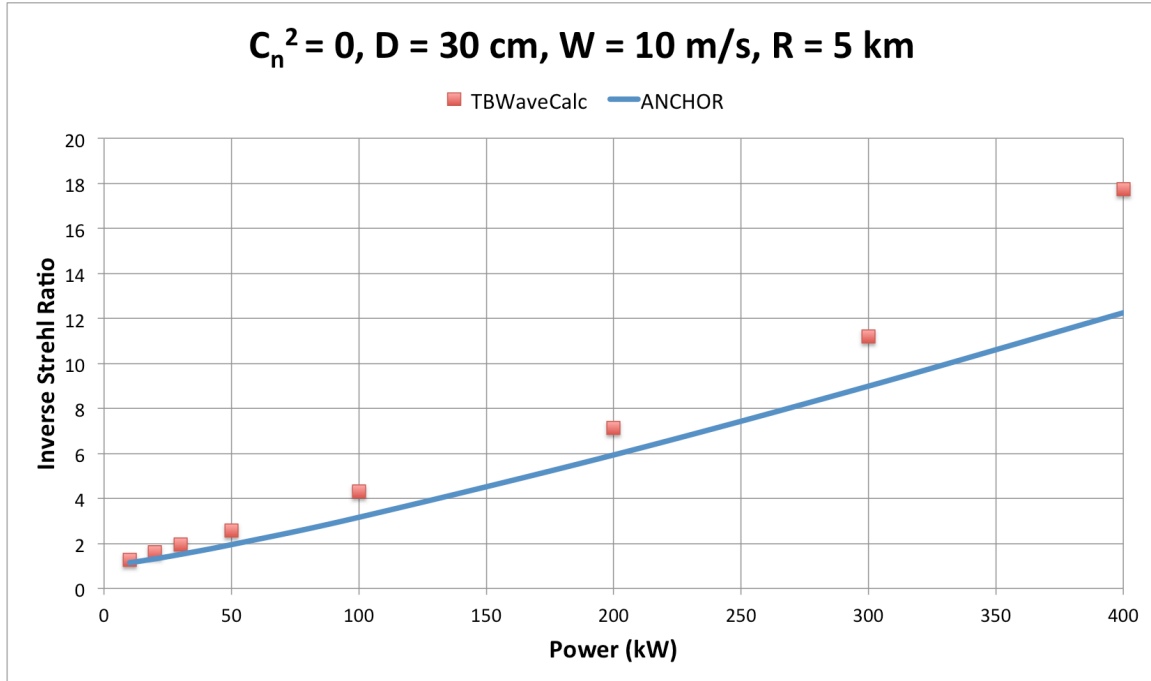
Figure 15. Inverse Strehl ratio plotted against laser output power for $C_n^2 = 0$

Figure 15 shows output power versus inverse Strehl ratio for $C_n^2 = 0$ (i.e., no turbulence). The plot shows that at low powers ANCHOR and TBWaveCalc compare well; however, at higher powers the variation is more noticeable with about a 30% difference.
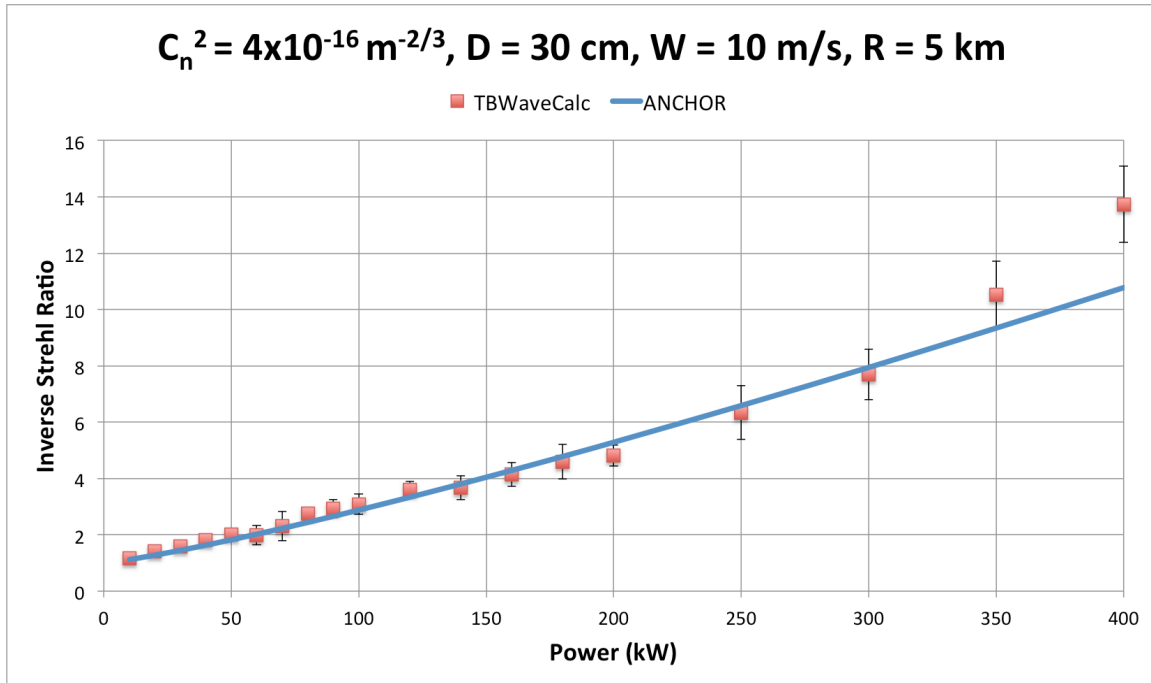
Figure 16. Inverse Strehl ratio plotted against laser output power for $C_n^2 = 4\text{x}10^{-16}$ $\text{m}^{-2/3}$

Figure 16 shows the output power versus inverse Strehl ratio for $C_n^2 = 4\text{x}10^{-16}$ $\text{m}^{-2/3}$. The plot shows that essentially, up to 400 kW, the ANCHOR results fall within a standard deviation—denoted by the error bars—of the TBWaveCalc results.
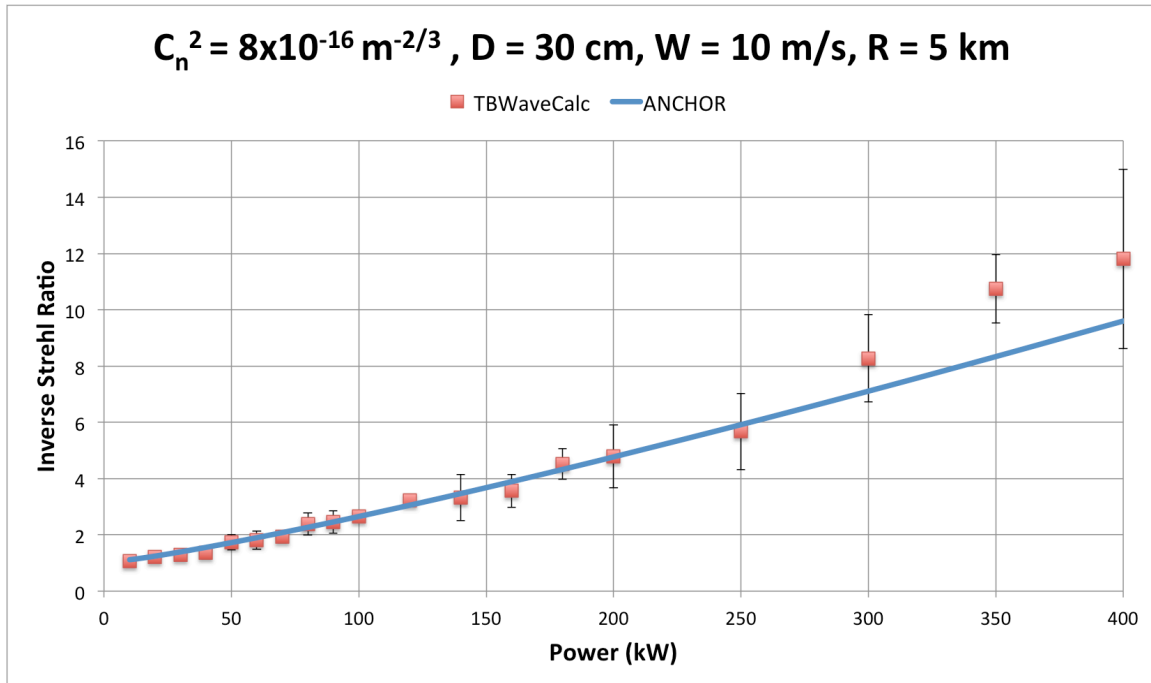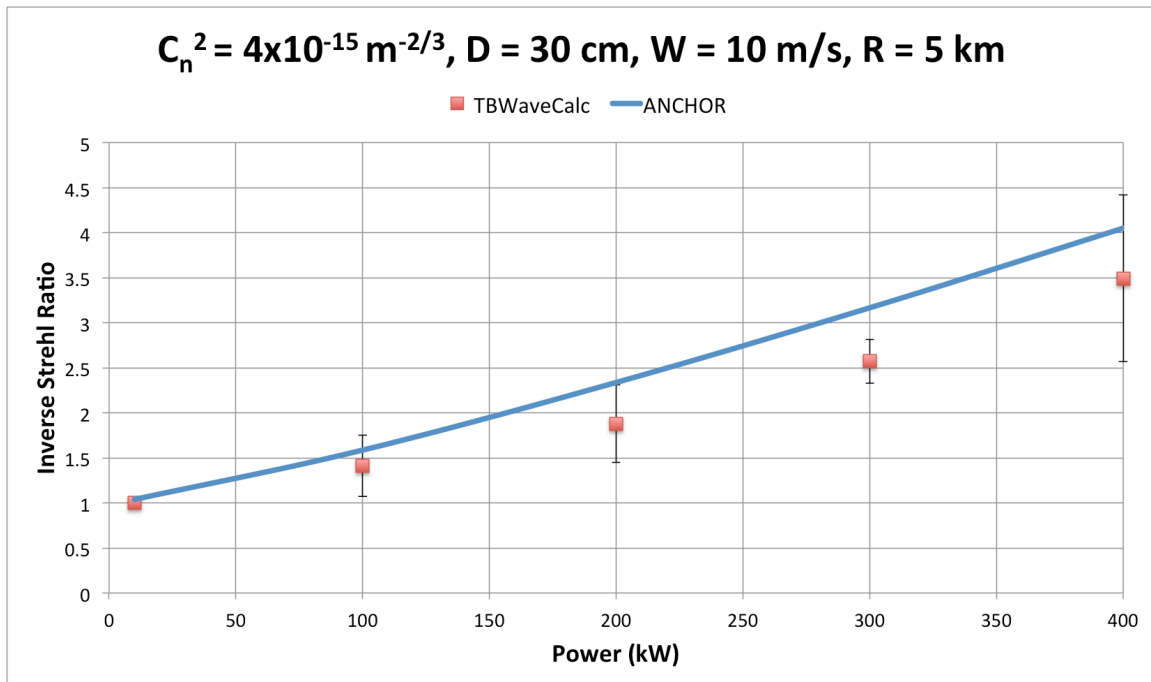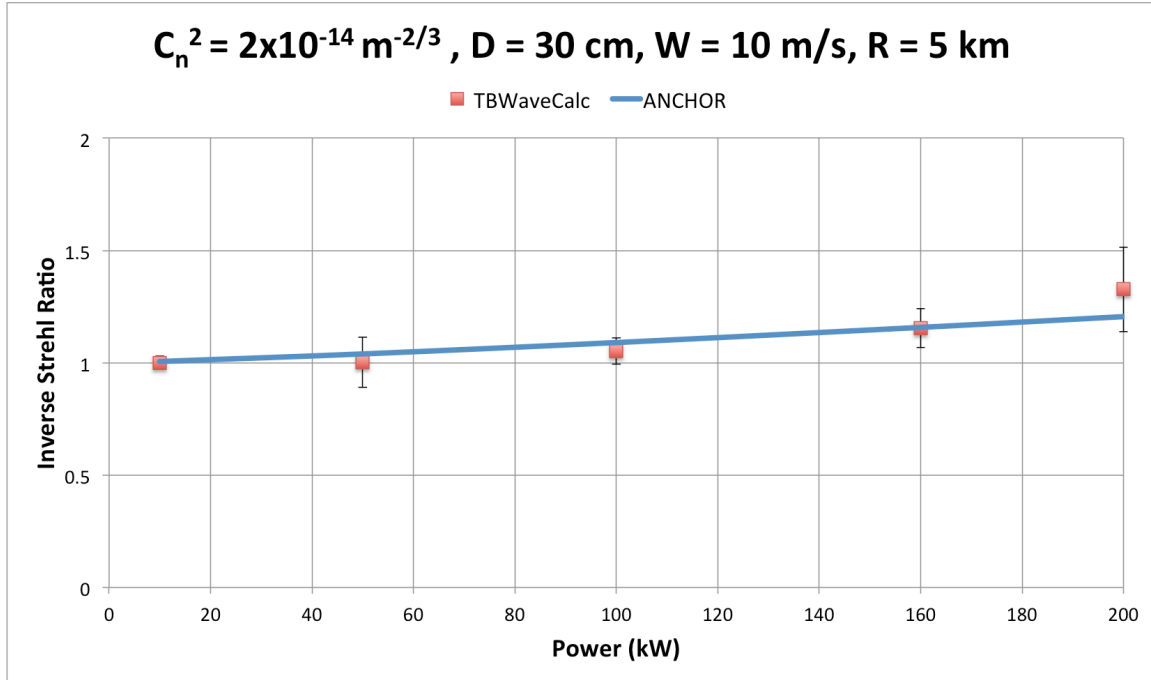
Figure 17. Inverse Strehl ratio plotted against laser output power for $C_n^2 = 8\text{x}10^{-16}$ $\text{m}^{-2/3}$

Figure 18. Inverse Strehl ratio plotted against laser output power for $C_n^2 = 4\text{x}10^{-15}$ $\text{m}^{-2/3}$
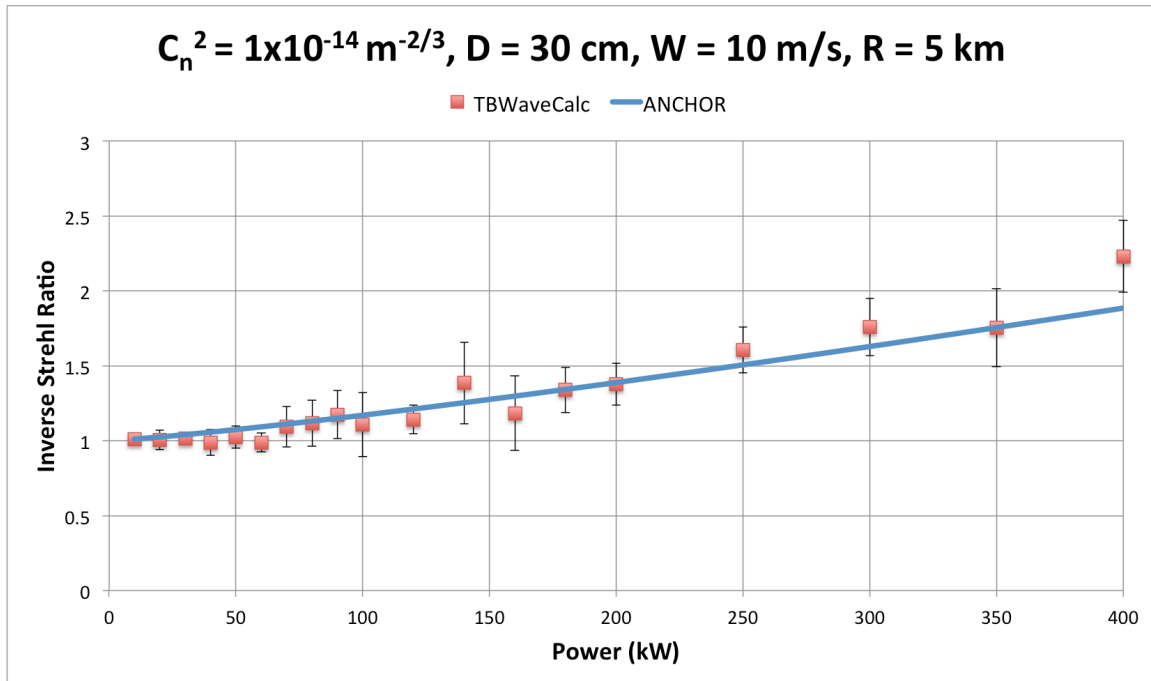
Figure 19. Inverse Strehl ratio plotted against laser output power for $C_n^2 = 1\text{x}10^{-14}$ m$^{-2/3}$
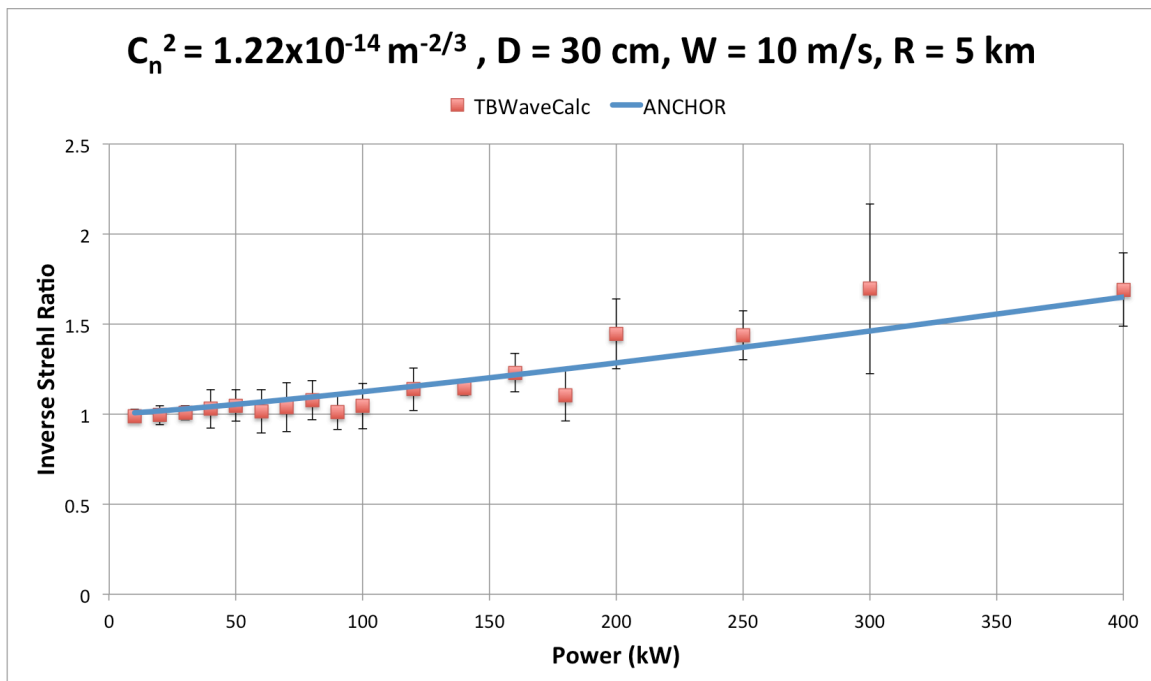
Figure 20. Inverse Strehl ratio plotted against laser output power for $C_n^2 = 1.22\text{x}10^{-14}$ m$^{-2/3}$

Figure 21. Inverse Strehl ratio plotted against laser output power for $C_n^2 = 2\text{x}10^{-14}$ $\text{m}^{-2/3}$

Figures 15–21 show output power versus inverse Strehl ratio for increasing turbulence in ascending order. At the power levels shown, these plots continue to show that the ANCHOR results compare well with TBWaveCalc, with ANCHOR's thermal blooming model falling within a standard deviation of the TBWaveCalc results. Figure 21 only shows output power from 10 to 200 kW and shows that at lower power levels the ANCHOR model agrees very well with TBWaveCalc. The general trend is that thermal blooming has a decreasing effect as turbulence becomes stronger; this happens because turbulence increases spot size, decreasing the irradiance.

2.   Results: Wind = 10 m/s, D = 30 cm, Slant Range = 5 km

Figures 22 and 23, using the same parameters for beam diameter and wind speed, compare the ANCHOR and TBWaveCalc results for a 5 km slant range where C_n^2 varies along the path as altitude increases.
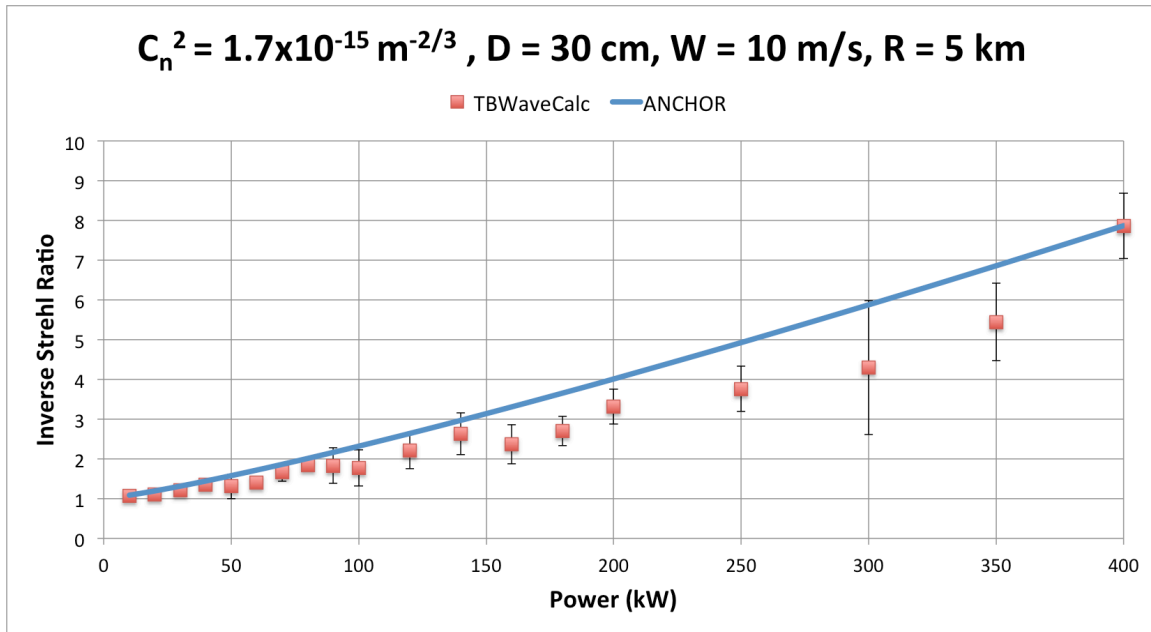
Figure 22. Inverse Strehl ratio plotted against laser output power for $C_n^2 = 1.7 \times 10^{-15}$ m$^{-2/3}$ at the surface and a target altitude of 100 m
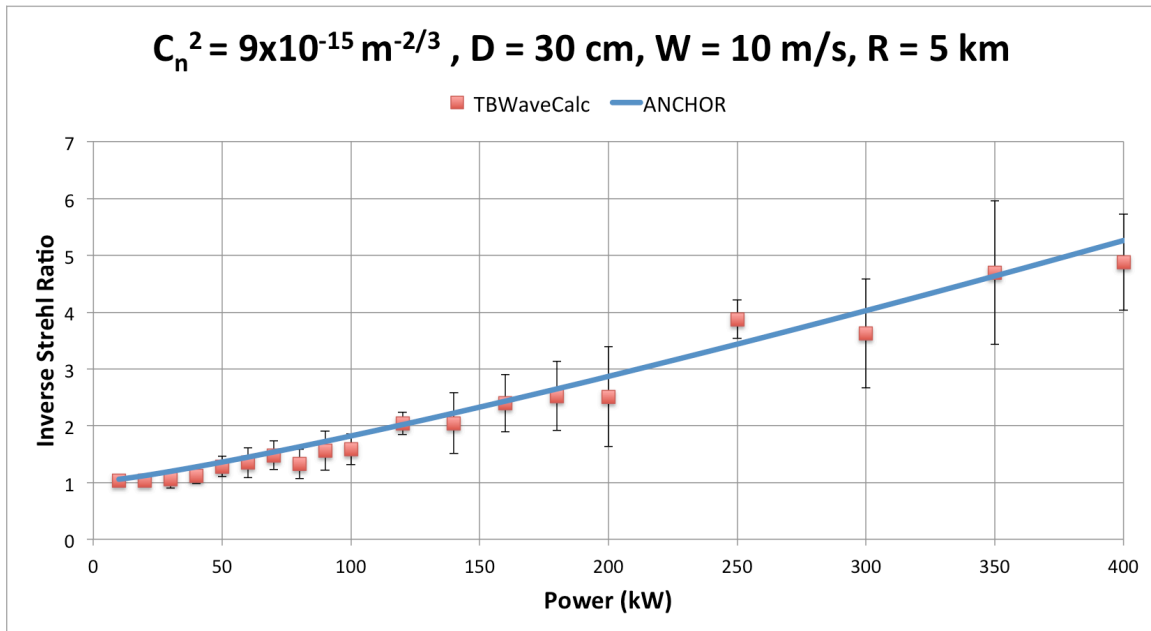

Figure 23. Inverse Strehl ratio plotted against laser output power for $C_n^2 = 9 \times 10^{-15}$ m$^{-2/3}$ at the surface and a target altitude of 1000 m

37

The plot shown in Figure 22 for a slant range with $C_n^2 = 1.7\text{x}10^{-15}$ m$^{-2/3}$ at the surface and a target altitude of 100 m, shows that ANCHOR's thermal blooming model is in agreement with TBWaveCalc. Likewise, Figure 23 with a profile $C_n^2 = 9\text{x}10^{-15}$ m$^{-2/3}$ at the surface and a target altitude of 1000 m also shows good agreement between ANCHOR and TBWaveCalc.

3.   Results: Wind = 5 m/s, D = 30 cm, Range = 5 km

In Figures 24 and 25, the inverse Strehl ratio is plotted against output laser power from 10 kW to 400 kW. The beam diameter at the source is 30 cm; the wind is a constant 5 m/s; the range is 5 km.
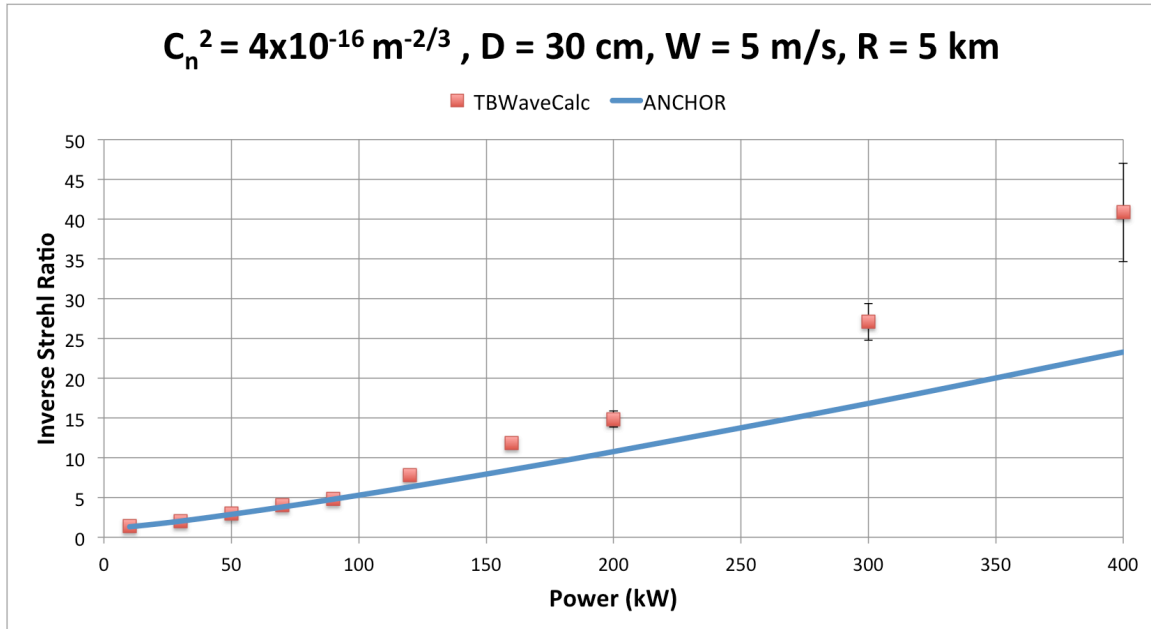
Figure 24. Inverse Strehl ratio plotted against laser output power for $C_n^2 = 4\text{x}10^{-16}$ m$^{-2/3}$
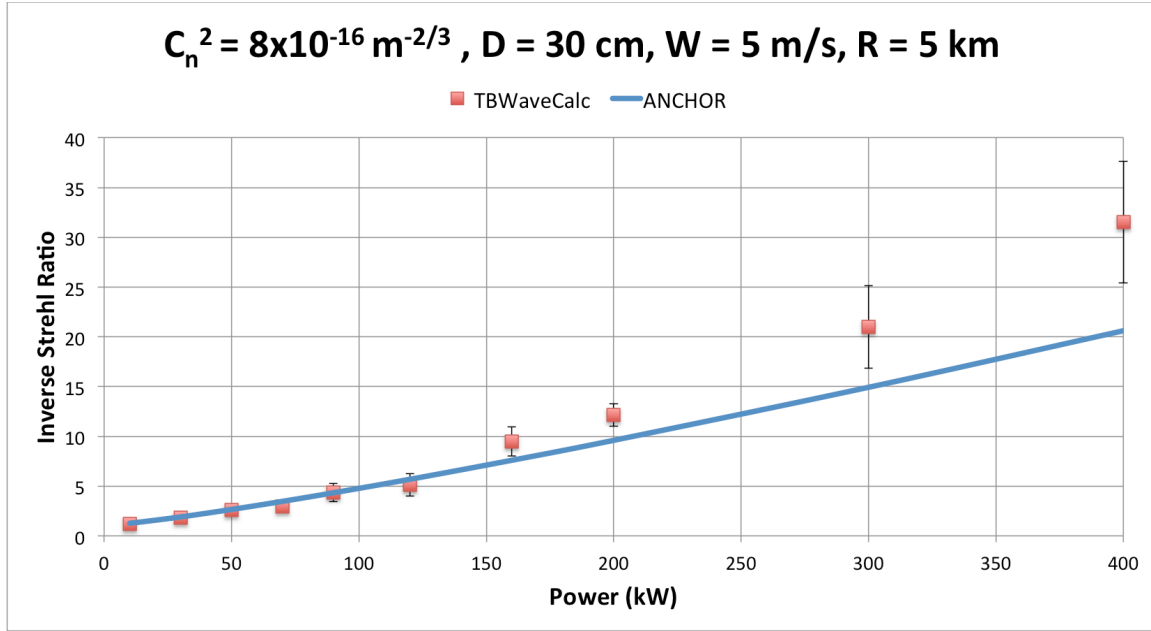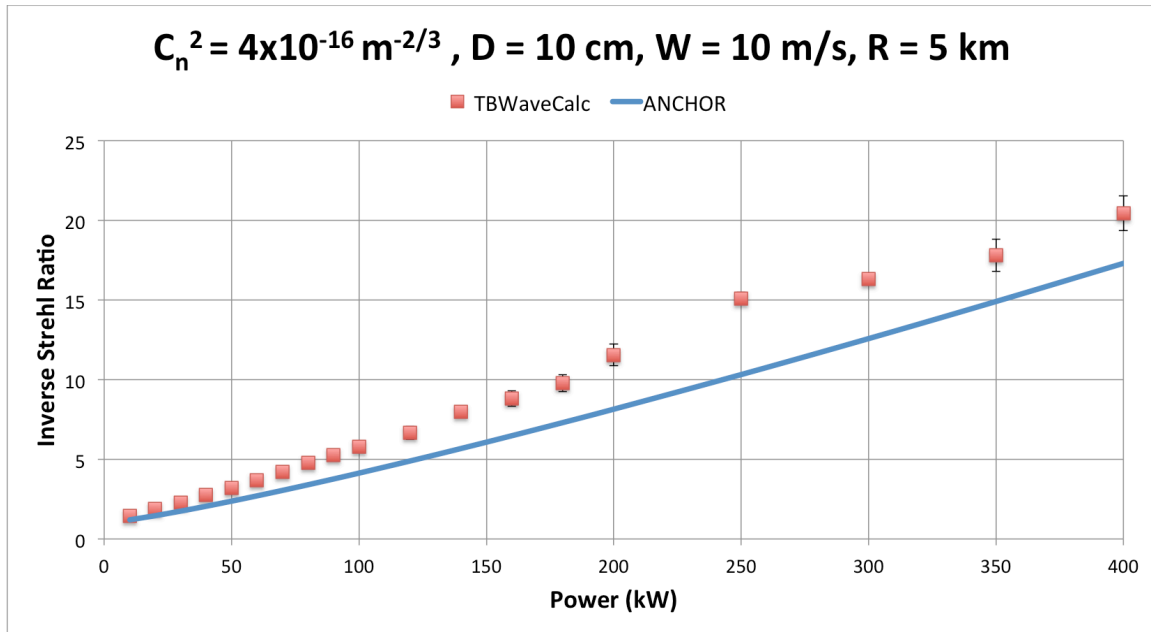
Figure 25. Inverse Strehl ratio plotted against laser output power for
$$C_n^2 = 8\text{x}10^{-16} \text{ m}^{-2/3}$$

For a light wind of 5 m/s, the ANCHOR thermal blooming model agrees well with TBWaveCalc for low powers but the deviation when turbulence is low is more noticeable at high powers.

4.   Results: Wind = 10 m/s, D = 10 cm, Range = 5 km

In Figures 26–29, the inverse Strehl ratio is plotted against output power from 10 kW to 400 kW. The beam diameter at the source is 10 cm; the wind is constant at 10 m/s; the range is 5 km.

Figure 26. Inverse Strehl ratio plotted against laser output power for $C_n^2 = 4\text{x}10^{-16}\ \text{m}^{-2/3}$
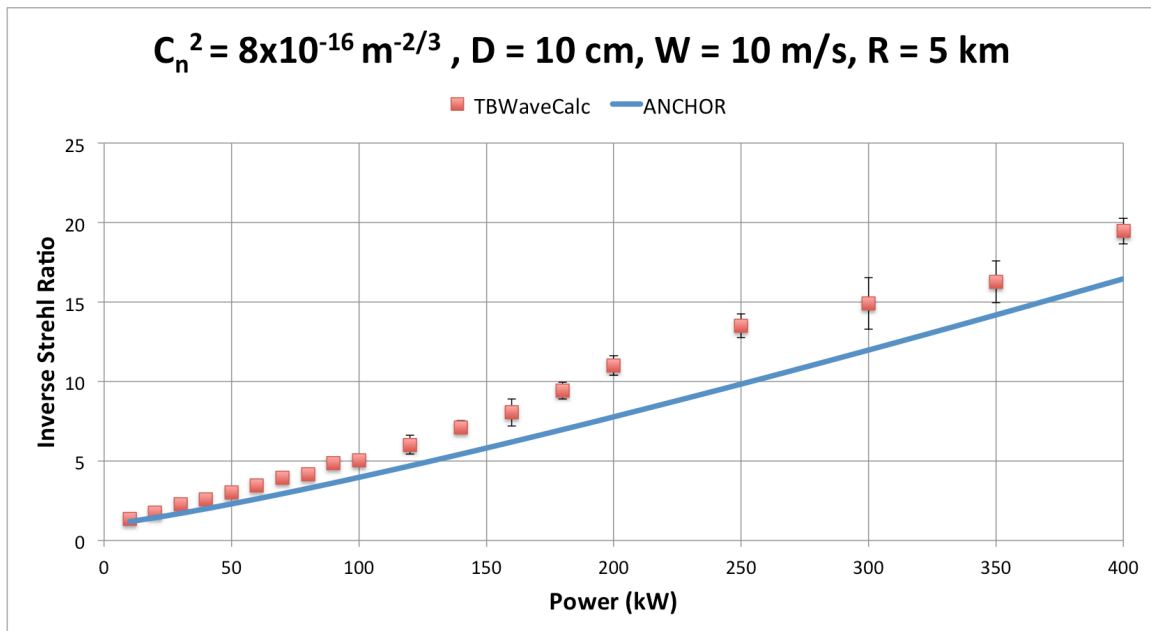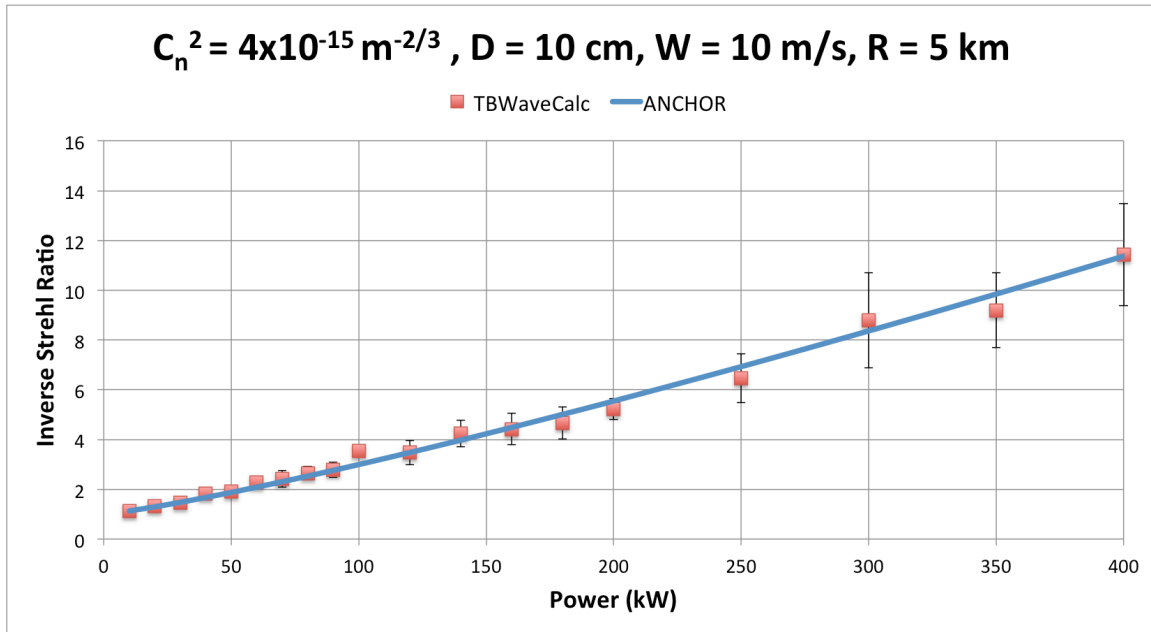

Figure 27. Inverse Strehl ratio plotted against laser output power for $C_n^2 = 8\text{x}10^{-16}\ \text{m}^{-2/3}$

Figure 28. Inverse Strehl ratio plotted against laser output power for
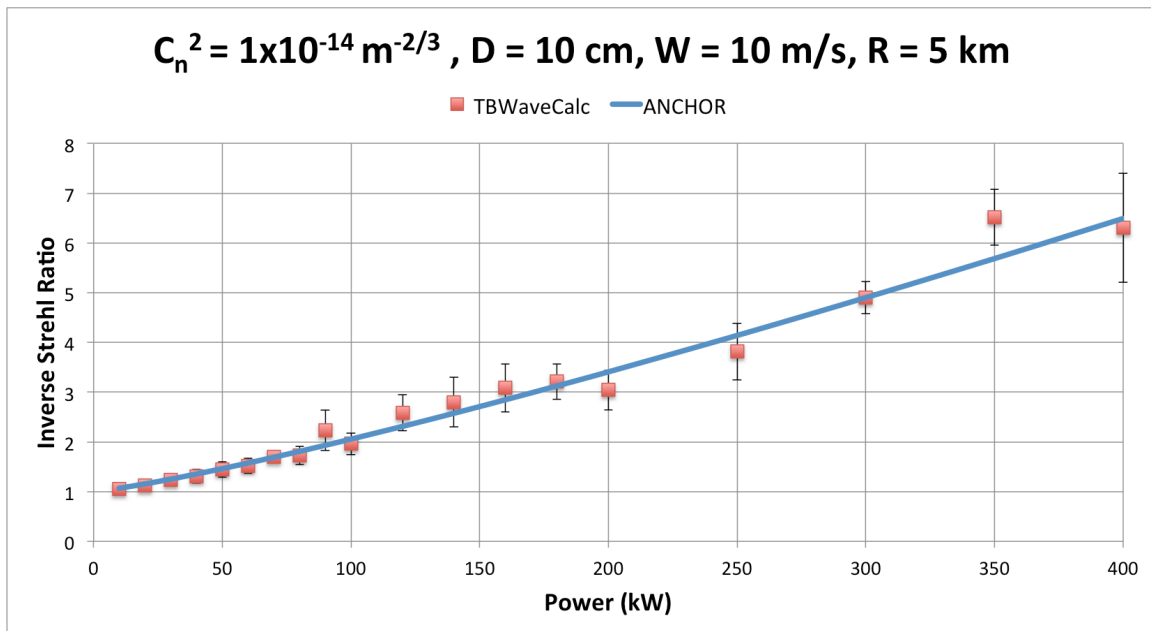$C_n^2 = 4\text{x}10^{-15}\ \text{m}^{-2/3}$

Figure 29. Inverse Strehl ratio plotted against laser output power for
$C_n^2 = 1\text{x}10^{-14}\ \text{m}^{-2/3}$

Figures 26–29 show that for a beam diameter at the source of 10 cm, ANCHOR and TBWaveCalc results agree very well for higher turbulence. The figures also show that for lower turbulence the ANCHOR results slightly underestimate the TBWaveCalc results.

5. Results: Wind = 10 m/s, D = 50 cm, Range = 5 km

For Figures 30–32, the inverse Strehl ratio is plotted against output power for a beam diameter of 50 cm, a constant wind of 10 m/s, and a range of 5 km.
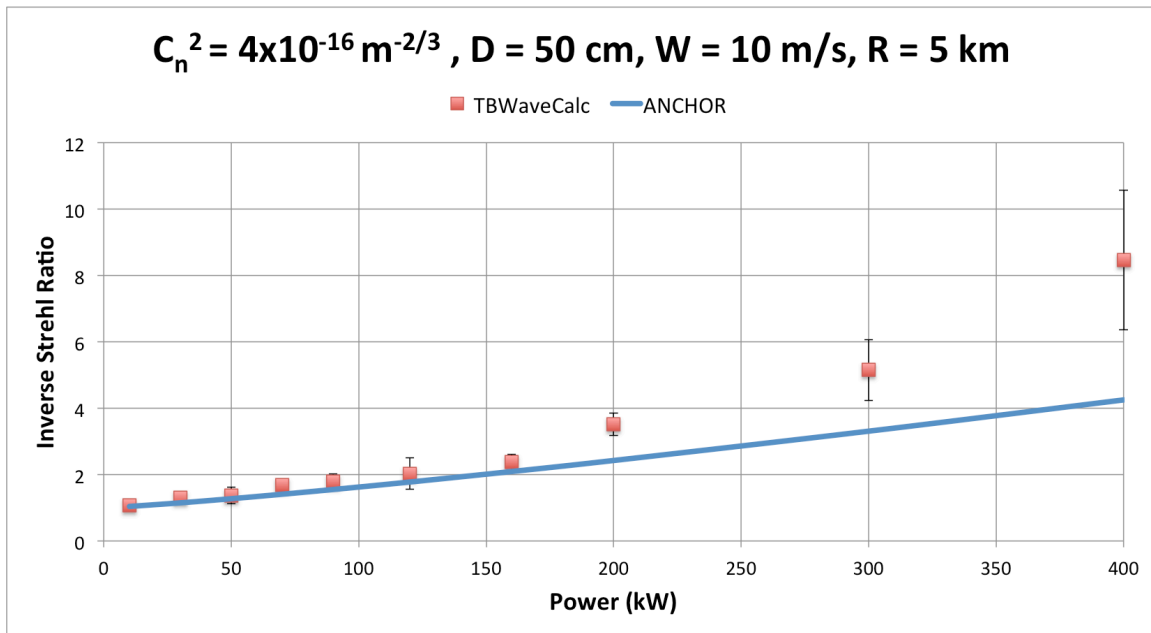

Figure 30. Inverse Strehl ratio plotted against laser output power for
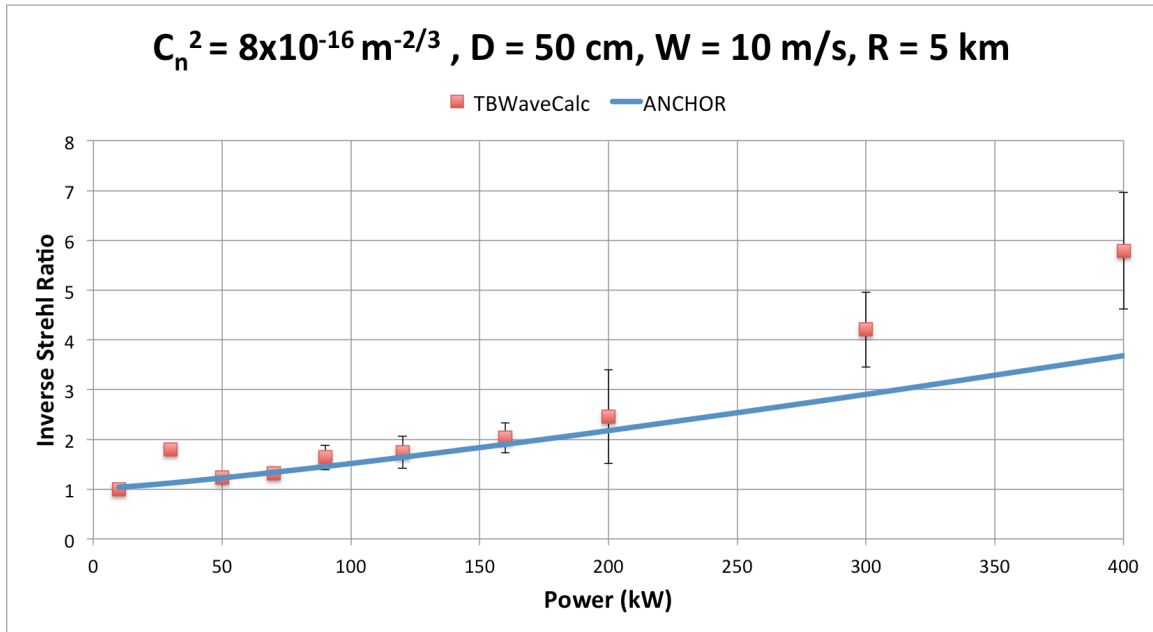$$C_n^2 = 4x10^{-16} \text{ m}^{-2/3}$$

Figure 31. Inverse Strehl ratio plotted against laser output power for $C_n^2 = 8 \times 10^{-16} \text{ m}^{-2/3}$
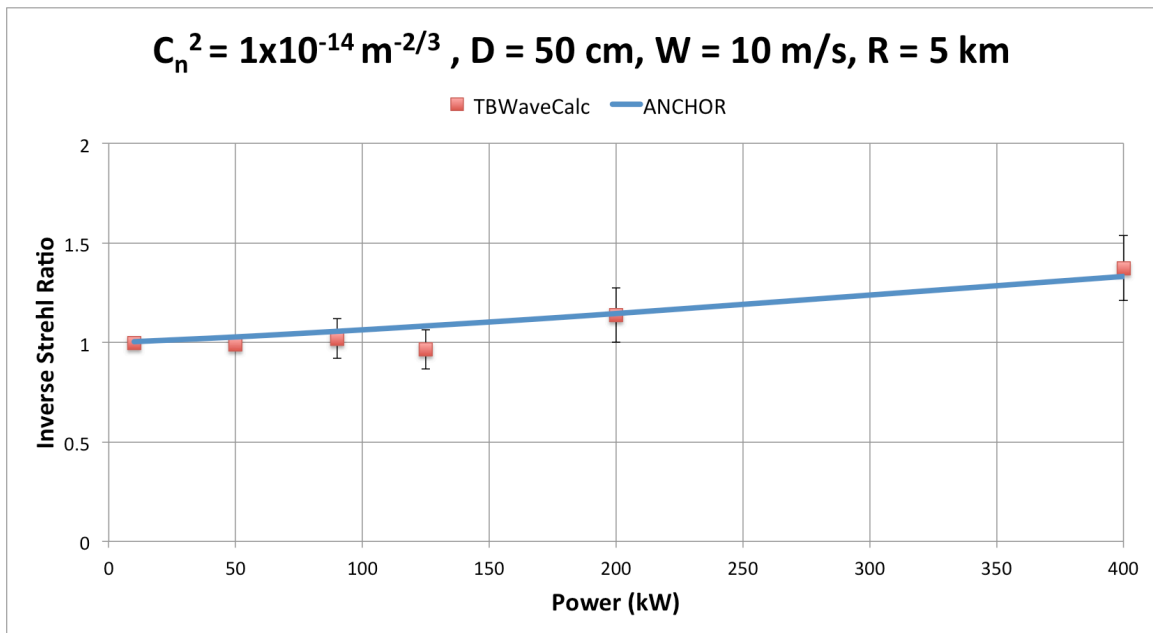

Figure 32. Inverse Strehl ratio plotted against laser output power for $C_n^2 = 1 \times 10^{-14} \text{ m}^{-2/3}$

Figures 30–32 show that the ANCHOR thermal blooming and TBWaveCalc results agree well for a beam diameter at the source of 50 cm in strong turbulence. Comparing the results in weak turbulence show the greatest variation at higher powers.

6. Results: Wind = 10 m/s, D = 30 cm, Range = 8 km

In Figures 33 and 34 the inverse Strehl ratio is plotted against output power for a beam diameter of 30 cm, a constant wind of 10 m/s, and a range of 8 km.
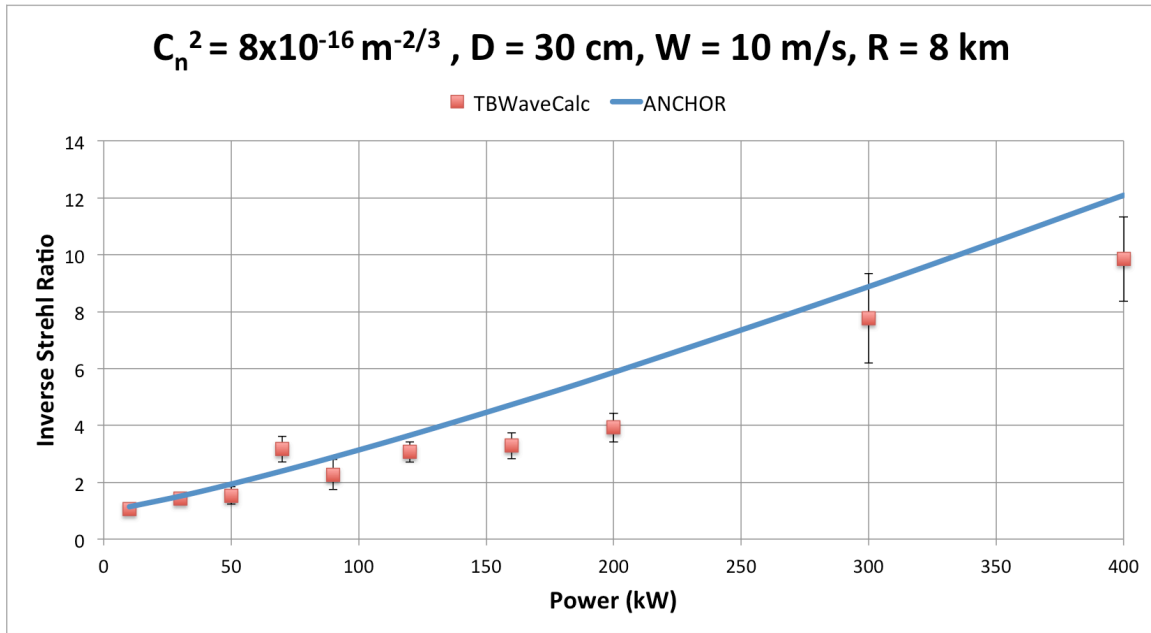

Figure 33. Inverse Strehl ratio plotted against laser output power for
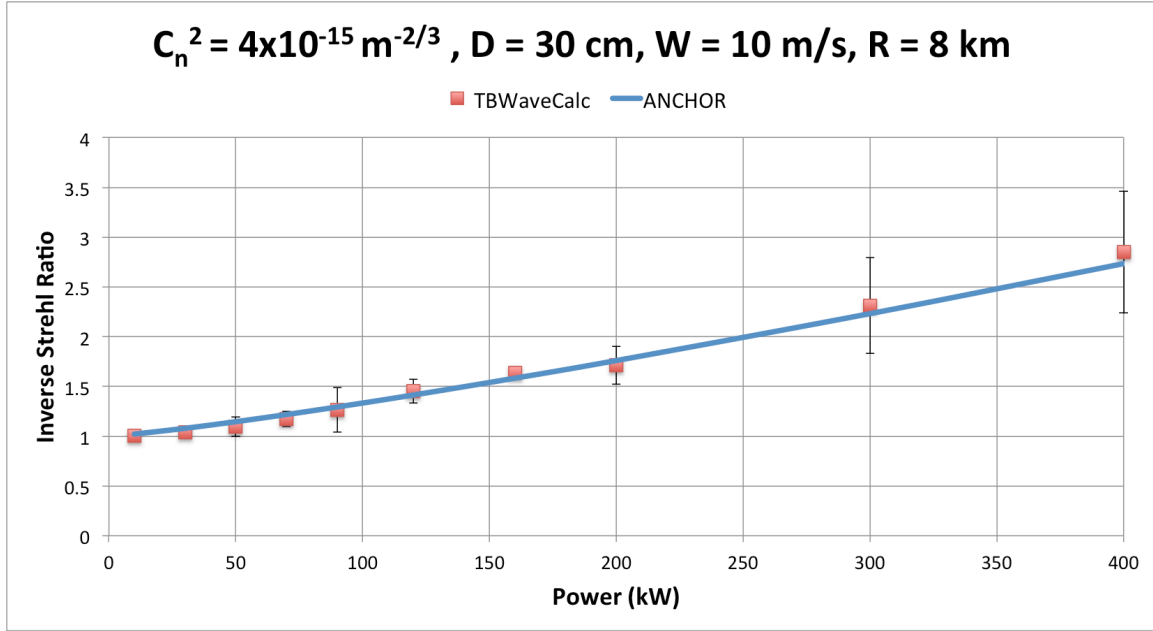$$C_n^2 = 8\text{x}10^{-16}\ \text{m}^{-2/3}$$

Figure 34. Inverse Strehl ratio plotted against laser output power for
$$C_n^2 = 4\mathrm{x}10^{-15} \ \mathrm{m}^{-2/3}$$

Figures 33 and 34 show that the ANCHOR model and the TBWaveCalc results agree well for a range of 8 km, showing almost no variation for $C_n^2 = 4\mathrm{x}10^{-15} \ \mathrm{m}^{-2/3}$ and good agreement within a standard deviation for $C_n^2 = 8\mathrm{x}10^{-16} \ \mathrm{m}^{-2/3}$.

7.   Results: Wind = 5 m/s, D = 30 cm, Range = 8 km

In Figure 35, the inverse Strehl ratio is plotted against output power for a beam diameter of 30 cm, a constant wind of 5 m/s, and a range of 8 km.
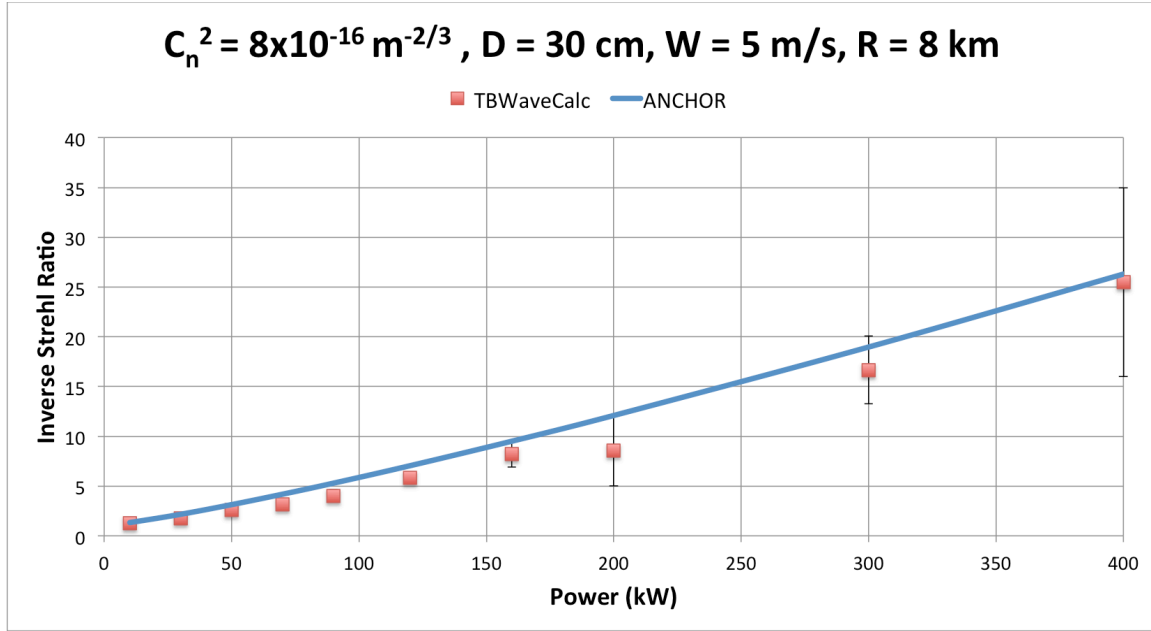
Figure 35. Inverse Strehl ratio plotted against laser output power for $C_n^2 = 8\mathrm{x}10^{-16}$ $\mathrm{m}^{-2/3}$

Comparing Figure 35 with Figure 33 shows that for $C_n^2 = 8\mathrm{x}10^{-16}$ $\mathrm{m}^{-2/3}$ the ANCHOR model agrees better with the TBWaveCalc for a wind speed of 5 m/s and a range of 8 km, with Figure 35 falling within one standard deviation of the TBWaveCalc results.

8.　　Results: Wind = 5 m/s, D = 30 cm, Range = 1 km

For Figures 36–38, the inverse Strehl ratio is plotted against output power for a beam diameter of 30 cm, a constant wind of 5 m/s, and a range of 1 km.
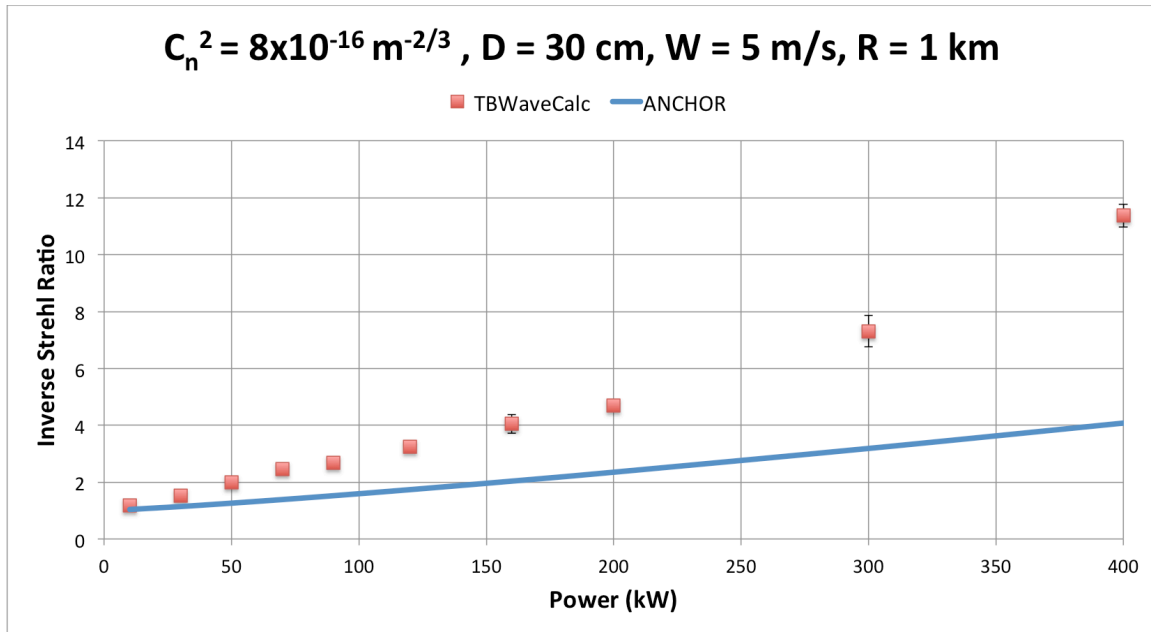
Figure 36. Inverse Strehl ratio plotted against laser output power for
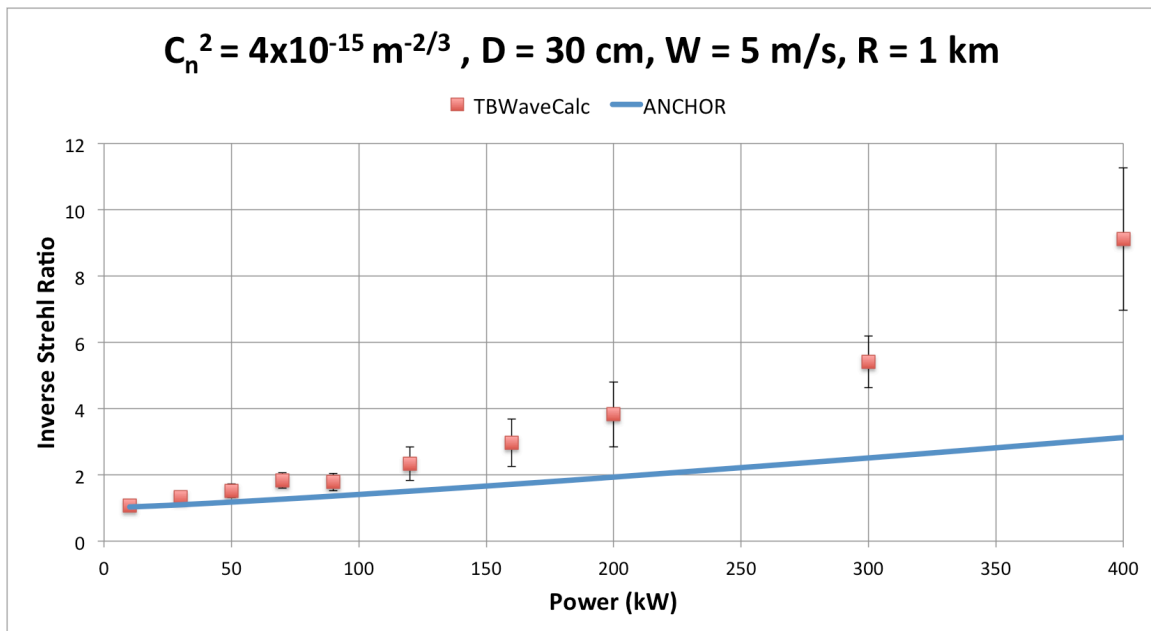$C_n^2 = 8\text{x}10^{-16}\text{ m}^{-2/3}$

Figure 37. Inverse Strehl ratio plotted against laser output power for
$C_n^2 = 4\text{x}10^{-15}\text{ m}^{-2/3}$

$$C_n{}^2 = 1\text{x}10^{-14}\ \text{m}^{-2/3}\ ,\ D = 30\ \text{cm},\ W = 5\ \text{m/s},\ R = 1\ \text{km}$$
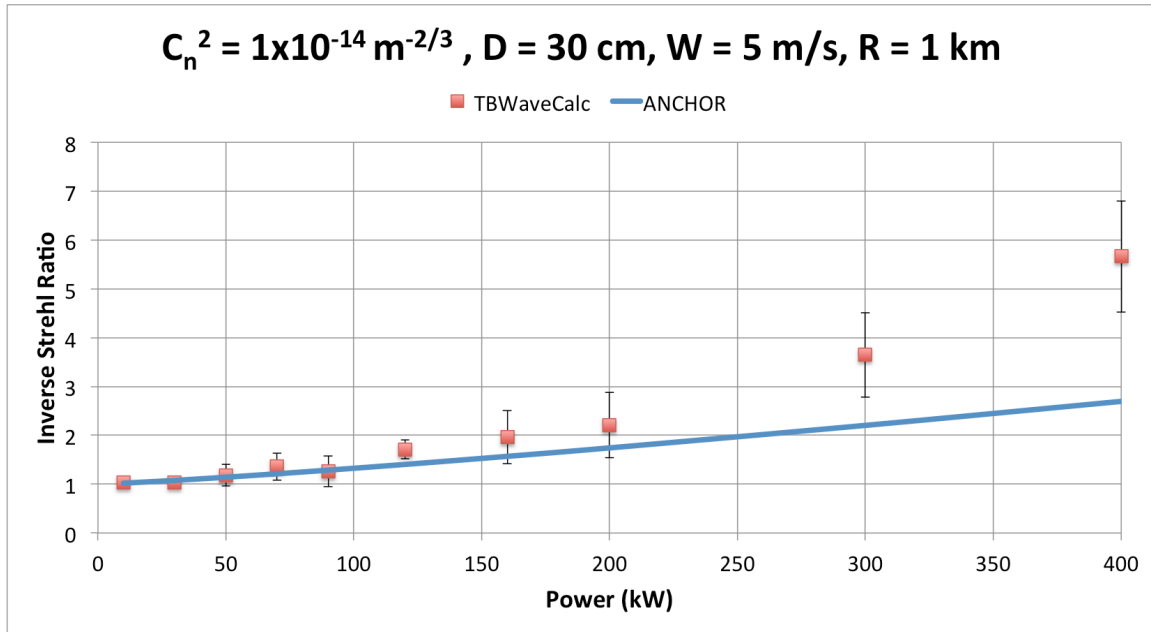
Figure 38. Inverse Strehl ratio plotted against laser output power for
$$C_n^2 = 1\text{x}10^{-14}\ \text{m}^{-2/3}$$

Figure 36–38 show that for a range of 1 km are in close agreement for low powers, however, for the turbulence profiles shown the ANCHOR model and TBWaveCalc results diverge for high powers within 1 km.

9.   Results: Wind = 20 m/s, D = 30 cm, Range = 5 km

For Figures 39–43, the inverse Strehl ratio is plotted against output power for a beam diameter of 30 cm, a constant wind of 20 m/s, and a range of 5 km.
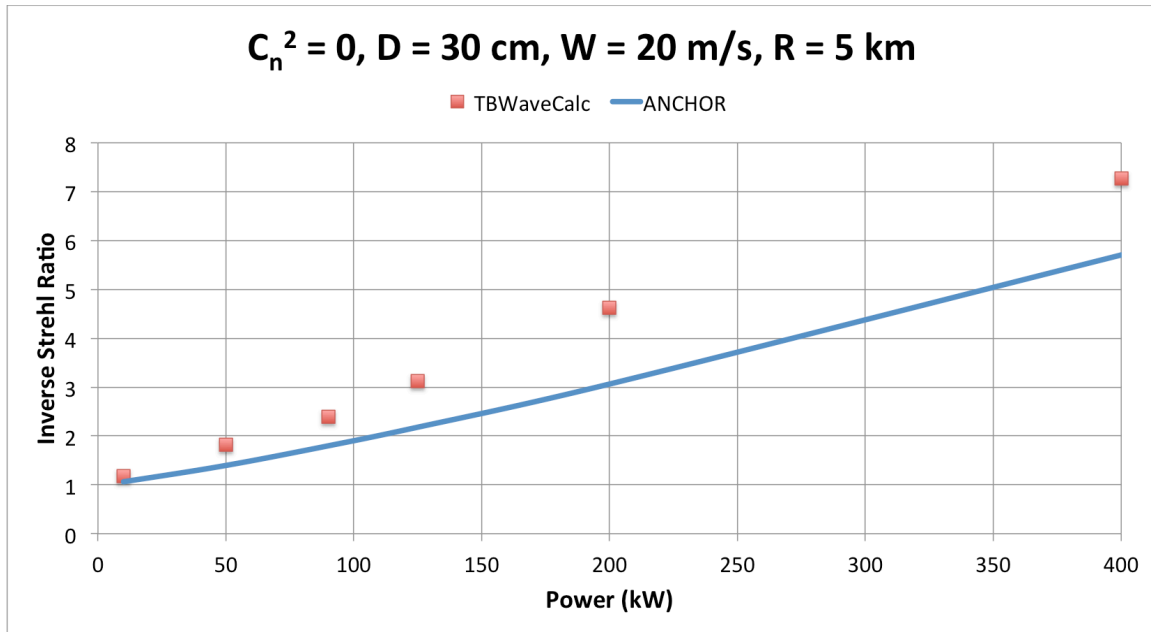
Figure 39. Inverse Strehl ratio plotted against laser output power for $C_n^2 = 0$
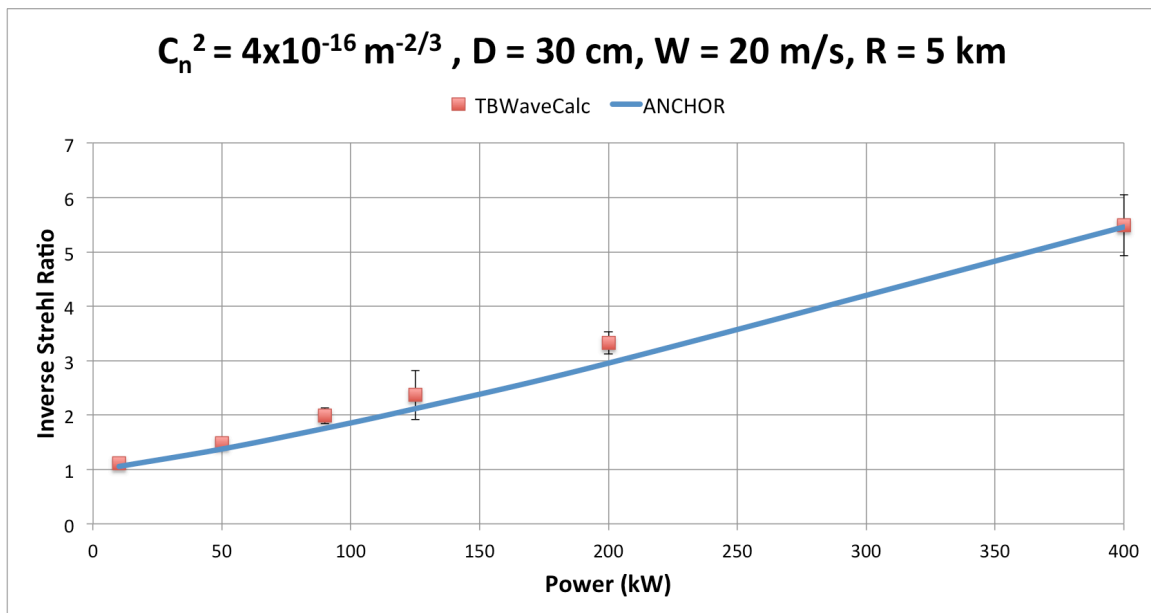

Figure 40. Inverse Strehl ratio plotted against laser output power for
$C_n^2 = 4\text{x}10^{-16} \text{ m}^{-2/3}$
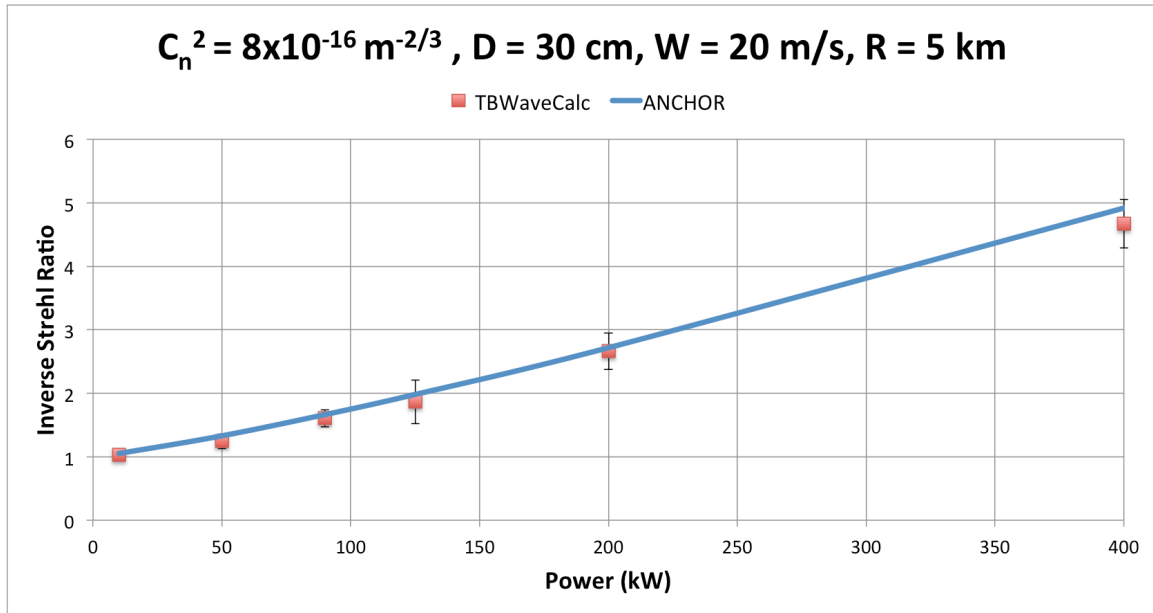
Figure 41. Inverse Strehl ratio plotted against laser output power for
$$C_n^2 = 8\text{x}10^{-16} \text{ m}^{-2/3}$$

Figure 42. Inverse Strehl ratio plotted against laser output power for
$$C_n^2 = 4\text{x}10^{-15} \text{ m}^{-2/3}$$

$C_n^2 = 1 \times 10^{-14}$ m$^{-2/3}$, D = 30 cm, W = 20 m/s, R = 5 km

■ TBWaveCalc ▬ ANCHOR
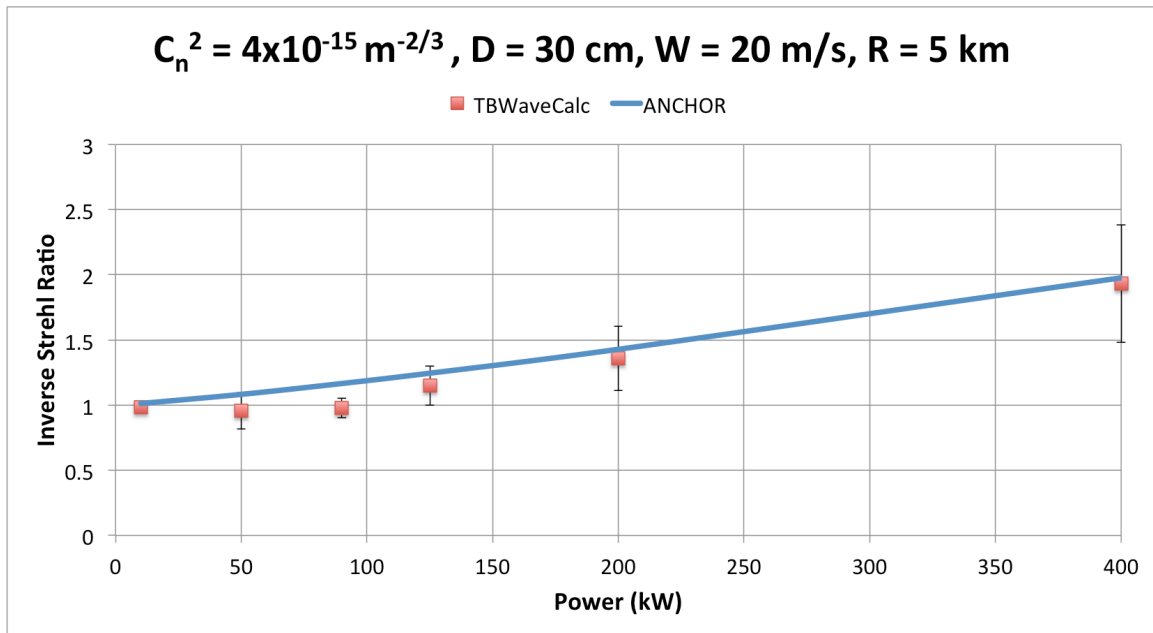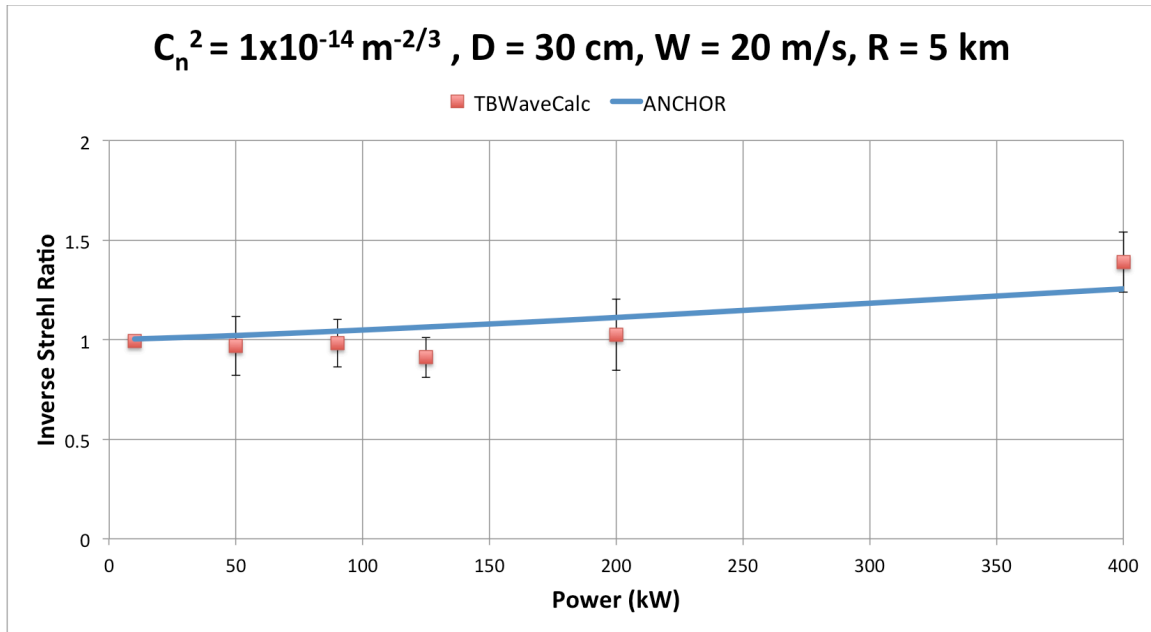
Figure 43. Inverse Strehl ratio plotted against laser output power for $C_n^2 = 1 \times 10^{-14}$ m$^{-2/3}$

Figures 39–43 show that for a constant wind speed of 20 m/s the ANCHOR model and TBWaveCalc results continue to agree well at higher turbulence with larger variation occurring at lower turbulence at higher power levels.

THIS PAGE INTENTIONALLY LEFT BLANK

V.   CONCLUSION

The focus of this thesis was the calibration of the ANCHOR thermal blooming model against TBWaveCalc in a variety of conditions for laser output powers from 10 kW to 400 kW. The results of that calibration, illustrated in the previous chapter, show that the ANCHOR model, which uses a simple analytical scaling formula, is in general agreement with most of the TBWaveCalc results after adjusting the coefficients of the scaling formula. The results also show that the correlation is particularly strong at lower output powers, however, showing noticeable deviations in the 300–400 kW range for smaller turbulence values. Deviation was also noted for lower wind velocities, as the differences at high powers increased markedly as wind velocity decreased from 10 m/s to 5 m/s. For higher turbulence values, ANCHOR and TBWaveCalc show good correlation across the results with the exception of the 1 km range. Overall, the updated ANCHOR thermal blooming model shows good agreement with TBWaveCalc.

More work can be done to further refine the ANCHOR thermal blooming model. Future work includes increasing the data set of TBWaveCalc results for better correlation with ANCHOR. Future projects can also be done in order to calibrate the ANCHOR thermal blooming model for a Gaussian profile.

THIS PAGE INTENTIONALLY LEFT BLANK

LIST OF REFERENCES

[1]   J. R. Albertine, "History of Navy HEL technology development and systems testing," in *Proceedings of SPIE 4632, Laser and Beam Control Technologies*, 2002, vol. 4632 pp. 32–37.

[2]   Focus like a laser. (2012, Jan. 16). cosmoscon. [Online]. Available: https://cosmoscon.com/2012/01/16/focus-like-a-laser/

[3]   G. P. Perram, S. J. Cusumano, R. L. Hengehold, and S. T. Fiorino, *An introduction to laser weapon systems.* Albuquerque, NM: Directed Energy Professional Society, 2010.

[4]   R. O'Rourke, "Navy shipboard lasers for surface, air, and missile defense: background and issues for Congress," Congressional Research Service, Washington, DC, Rep. 7-5700, June 1, 2015.

[5]   WaveTrain anchoring and validation. (n.d.). MZA Associates Corporation. [Online]. Available: https://mza.com/doc/wavetrain/anchor/index.htm. Accessed: Apr. 5, 2016.

[6]   F. G. Gebhardt, "High power laser propagation," *Applied Optics*, vol. 15, no. 6, Jun. 1976.

[7]   D. L. Fried, "Optical resolution through a randomly inhomogeneous medium for very long and very short exposures," *J. Opt. Soc. Am.*, vol. 56, no. 10, pp. 1372–1379, 1966.

[8]   H. Breaux, W. Evers, R. Sepucha, and C. Whitney, "Algebraic model for cw thermal-blooming effects," *Appl. Opt. Applied Optics*, vol. 18, no. 15, pp. 2638–2644, Jan. 1979.

[9]   P. S. Guest and T. Murphree, "Modeling and Simulating Environmental Effects," in *MOVES Research and Education Systems Seminar*, Aug. 1, 2012.

[10]   P. Frederickson et al., "Estimating the refractive index structure parameter (C_n^2) over the ocean using bulk methods," *J. Appl. Meteorology*, vol. 39, pp. 1770–1783, Oct. 2000.

[11]   *LEEDR User Guide*, 3rd ed. AFIT, Wright-Patterson Air Force Base, OH, 2013.

[12]   COAMPS version 3 model description. (n.d.). Naval Research Lab. [Online]. Available at: http://www.nrlmry.navy.mil/coamps-web/web/docs. Accessed: Apr. 20, 2016.

[13]   F. Zhang, and Y Li, "The scaling laws for thermal blooming of the high-energy laser propagation," in *Proceedings of SPIE 5832 Optical Technologies for Atmospheric, Ocean, and Environmental Studies*, 2005, vol. 5832 pp. 25-30.

[14]   F. G. Gebhardt, "Twenty-five years of thermal blooming: An overview," in *Proceedings of SPIE 1221 Propagation of High-Energy Laser Beams Through the Earth's Atmosphere*, 1990, vol. 1221 pp. 2-25.

[15]   A. M. Ngwele and M. R. Whiteley, "Scaling law modeling of thermal blooming in wave optics," in *DEPS Directed Energy Symposium*, Nov. 2, 2006.

[16]   E.P. Magee and A.M. Ngwele. (2013). ATMTools: A toolbox for atmospheric propagation modeling [Online]. Available: http://scalingcodes.mza.com/doc/AtmToolsUserGuide.pdf

INITIAL DISTRIBUTION LIST

1.   Defense Technical Information Center
        Ft. Belvoir, Virginia

2.   Dudley Knox Library
        Naval Postgraduate School
        Monterey, California